

# Stochastic Exploration of Real Varieties via Variety Distributions

David Kahle\*

Jonathan D. Hauenstein†

October 22, 2024

## Abstract

Nonlinear systems of polynomial equations arise naturally in many applied settings, for example loglinear models on contingency tables and Gaussian graphical models. The solution sets to these systems over the reals are often positive dimensional spaces that in general may be very complicated yet have very nice local behavior almost everywhere. Standard methods in real algebraic geometry for describing positive dimensional real solution sets include cylindrical algebraic decomposition and numerical cell decomposition, both of which can be costly to compute in many practical applications. In this work we communicate recent progress towards a Monte Carlo framework for exploring such real solution sets. After describing how to construct probability distributions whose mass focuses on a variety of interest, we describe how Hamiltonian Monte Carlo methods can be used to sample points near the variety that may then be moved to the variety using endgames. We conclude by showcasing trial experiments using practical implementations of the method in the Bayesian engine **Stan**.

## 1 Introduction and background

In this article we consider stochastic methods to explore real algebraic varieties, solution sets of systems of algebraic equations. Such systems arise naturally throughout applied science, including statistical science where they can be seen in areas such as (conditional) independence and graphical models, regression and regression-like analyses, and the design of experiments.

As in all areas of mathematics, a bit of notation is required to orient oneself with the relevant concepts. Let  $k$  denote a field,  $k^n$  the  $n$ -dimensional affine/coordinate vector space of  $n$ -tuples of elements of  $k$ ,  $k[\mathbf{x}] = k[x_1, x_2, \dots, x_n]$  the commutative ring of polynomials in the  $n$  variables  $x_1, \dots, x_n$  with coefficients from  $k$ , and  $g_1, \dots, g_m \in k[\mathbf{x}]$   $m$  polynomials in  $k[\mathbf{x}]$ , collectively denoted  $\mathbf{g} = [g_i]_{i=1}^m \in k[\mathbf{x}]^m$ . The variety  $\mathcal{V}(\mathbf{g}) = \mathcal{V}(g_1, \dots, g_m)$  defined by the polynomials  $g_1, \dots, g_m$ , sometimes called an algebraic set, is the collection of points

$$\mathcal{V}(\mathbf{g}) = \mathcal{V}(g_1, \dots, g_m) = \{\mathbf{x} \in k^n : g_1(\mathbf{x}) = g_2(\mathbf{x}) = \dots = g_m(\mathbf{x}) = 0\} = \{\mathbf{x} \in k^n : \mathbf{g}(\mathbf{x}) = \mathbf{0}_m\}.$$

It is the solution set to the  $m \times n$  system of equations described by  $g_1, \dots, g_m$ . If  $m = n$ , so that the number of equations and unknowns is the same, the system is said to be square.

Polynomials can be viewed from two complimentary perspectives, first as symbolic objects among which operations are defined and second as functions. Every polynomial  $g \in k[\mathbf{x}]$  is an expression of the form  $g = \sum_{\alpha \in \mathcal{A}} \beta_{\alpha} \mathbf{x}^{\alpha}$ , where  $\mathbf{x}^{\alpha} = \prod_{i=1}^n x_i^{\alpha_i}$  is monomial notation,  $\mathcal{A} \subset \mathbb{N}^n$ , and  $|\mathcal{A}| = b < \infty$  elements so that  $g$  has  $b$  terms. We refer to  $\mathbf{x}^{\alpha}$  as a monomial; that is, the product of powers of the variables without the coefficient. As convenient, we write polynomials in different ways:  $g = \sum_{\alpha \in \mathcal{A}} \beta_{\alpha} \mathbf{x}^{\alpha} = \sum \beta_{\alpha} \mathbf{x}^{\alpha} = \beta' \mathbf{x}^{\mathcal{A}} =$

\*Associate Professor, Department of Statistical Science, Baylor University. [david\\_kahle@baylor.edu](mailto:david_kahle@baylor.edu)

†Professor, Department of Applied and Computational Mathematics and Statistics, University of Notre Dame. [hauenstein@nd.edu](mailto:hauenstein@nd.edu)

$g(\mathbf{x}|\beta)$ , where  $\beta$  and  $\mathbf{x}^{\mathcal{A}}$  have  $b$  elements, the latter being the vector of monomials in  $\mathbf{x}$  with powers given by the elements of  $\mathcal{A}$ , which are assumed to have some order by convention. The (total) degree of a polynomial is the maximum sum of such powers over the terms of the polynomial,  $d = \max_{\alpha \in \mathcal{A}} \sum_{i=1}^n \alpha_i$ . Vectors of polynomials  $\mathbf{g} \in k[\mathbf{x}]^m$  can be referred to similarly, namely  $\mathbf{g} = \mathbf{g}(\mathbf{x}|\mathbf{B}) = \mathbf{B}\mathbf{x}^{\mathcal{A}}$ , where  $\mathbf{B} \in \mathbb{R}^{m \times b}$  is some real-valued matrix whose rows are indexed by the polynomials  $g_1, \dots, g_m$ , constituted of  $b_1, \dots, b_m$  terms respectively, and whose  $b$  columns are indexed by the elements of  $\mathcal{A}$ , whose cardinality is  $|\mathcal{A}| = b$ . These are the unique monomials of the pooled collection of  $g_i$ 's monomials.

In addition to expressions, polynomials can also be viewed as functions  $g : k^n \rightarrow k$  by substituting values of vectors  $\mathbf{x} \in k^n$  into the expression  $g$  and evaluating. In this setting, the variety of  $g$ ,  $\mathcal{V}(g)$ , corresponds to the zero level set of the hypersurface defined by  $g$ . Vectors of polynomials  $\mathbf{g} \in k[\mathbf{x}]^m$  are similarly considered from either perspective; functionally they are of the form  $\mathbf{g} : k^n \rightarrow k^m$ , i.e. vector fields. From this perspective, varieties can be seen to be intersections of zero level sets of polynomials, the individual varieties  $\mathcal{V}(g_i)$ . By definition, points  $\mathbf{x} \in \mathcal{V}(\mathbf{g}) \subseteq k^n$  are on the variety if and only if they satisfy the algebraic system of equations  $g_1(\mathbf{x}) = 0, \dots, g_m(\mathbf{x}) = 0$ .

The field of algebraic geometry investigates the duality of varieties (geometric objects) and ideals of  $k[\mathbf{x}]$  (algebraic objects). For example, if  $k$  is an algebraically closed field, there is an elegant bijective correspondence between certain ideals and varieties that enables geometric questions to be reformulated as algebraic ones and vice versa [Cox et al., 1997]. A common choice for  $k$  in algebraic geometry is thus  $k = \mathbb{C}$ , as  $\mathbb{C}$  is an algebraically closed field; however, in applications typically  $k = \mathbb{R}$  or more likely a computer representation of it. In this work we generally assume  $k = \mathbb{R}$  so that  $\mathcal{V}(\mathbf{g}) \subseteq \mathbb{R}^n$  and the coefficients of the polynomials are real. As a concrete example, suppose  $g_1 = x^2 + y^2 + z^2 - 1$  and  $g_2 = z - (x^2 + y^2)$  in  $\mathbb{R}[x, y, z]$ . A corresponding system of equations may be

$$\begin{aligned} x^2 + y^2 + z^2 &= 1 \\ x^2 + y^2 &= z, \end{aligned}$$

and  $\mathcal{V}(\mathbf{g})$  is the intersection of  $\mathcal{V}(g_1)$ , the unit sphere  $\mathcal{S}^2$  in  $\mathbb{R}^3$ , and  $\mathcal{V}(g_2)$ , the upward opening paraboloid in  $\mathbb{R}^3$ , which is a circle in  $\mathbb{R}^3$  hovering above the  $xy$ -plane. Such varieties can also be considered to be the real components of varieties of polynomials with real coefficients over  $\mathbb{C}^n$ . Notice that when  $k = \mathbb{R}$ , every variety can be generated by a single polynomial  $g = \mathbf{g}'\mathbf{g} = \sum_{i=1}^m g_i^2$ , since  $\mathbf{x} \in \mathcal{V}(\mathbf{g}) \iff (\forall i = 1, \dots, m)(g_i(\mathbf{x}) = 0) \iff \sum_{i=1}^m g_i(\mathbf{x})^2 = 0$ .

Varieties generalize the geometry of linear algebra in interesting and complex ways relevant to statistical science. In the linear case, polynomials are of total degree at most one, and the varieties are linear varieties that are either (1) empty, (2) consist of a single point, or (3) consist of a hyperplane of points. In the general setting,  $\mathcal{V}(\mathbf{g})$  may be (1) empty, (2) consist of a finite number of points (roots)  $\mathbf{x}_1, \dots, \mathbf{x}_r$ , in which case it is said to be zero-dimensional, or (3) consist of hypersurface(s) of points, in which case it is said to be positive dimensional. If  $g = 0$ , then the entire ambient space is a variety. Positive dimensional varieties are locally  $C^\infty$  manifolds almost everywhere [Bochnak et al., 1991], but otherwise can be quite complex: they can be disconnected, of varying dimension, and exhibit cusp-like and self-intersecting singularities. Varieties also form the closed sets of a topology called the Zariski topology: by taking products of the respective generating polynomials, unions of varieties are varieties, and by pooling the polynomials, intersections of varieties are varieties as well. In nice settings varieties can be decomposed into unions of irreducible pieces, each varieties themselves, called components. A variety is irreducible if, when represented as a union of distinct varieties, it is one of the varieties in the decomposition. An example is  $\mathcal{V}((x^2 + y^2)z)$ , which is the union of the irreducible varieties the  $z$ -axis  $\mathcal{V}(x^2 + y^2)$  and the  $xy$ -plane  $\mathcal{V}(z)$ . Varieties arise in naturally in many domains of statistics, typically as either subsets of parameter spaces defining models (e.g. independence models in contingency tables and Gaussian graphical models) or as response surfaces as in regression models, and these are a major topic of interest in algebraic statistics.

Being able to computationally understand varieties is a fundamental problem of applied mathematics: it corresponds to the ability to find solutions to systems of algebraic equations, generalizing linear algebra. Consequently, varieties have been investigated, as solution sets of systems of polynomial equations, for centuries. In algebraic geometry, in the 20th century two major lines of innovation surfaced specifically tailored

to these kinds of problems: symbolic methods based on Gröbner bases of ideals and numerical methods based on homotopy continuation [Sturmfels, 2002]. The first approach is a generalization of the Gaussian elimination/back substitution algorithm of linear algebra and is able to provide closed form solutions to the system in the zero-dimensional case, where closed form is understood in the sense that the original system is reformulated as a hierarchy of univariate polynomial root-finding problems, which can be efficiently and accurately computed numerically [Cox et al., 2015]. The challenge with this strategy is that the reformulation of the problem, the computation of a Gröbner basis, is well-known to have worst-case behavior that is double exponential time, so for practical purposes the methods in general must be assumed to be infeasible [Mayr and Meyer, 1982].<sup>1</sup> The second numerical approach is a clever iterative application of predictor-corrector methods: one forms a homotopy from the solution set of a known system into that of the target system and carefully tracks the solution set through the homotopy numerically. The algebraic structure of the problem can be exploited to guarantee that the process is accurate and fast with certifiable solutions when properly initialized [Sommese and Wampler, 2005]. While the method works well in a broad array of practical applications and is implemented in software such as Bertini(2), PHCpack, Mathematica, and others, the method, and consequently the software, is not designed to *explore* positive dimensional varieties [Bates et al., 2013, Verschelde, 1999]. Similarly, they are designed to work over  $\mathbb{C}^n$ , not  $\mathbb{R}^n$ . Still more recent methods sample a variety by carefully moving a linear space through the variety [Breiding and Marigliano, 2020]. By contrast, the methods described in this article use novel probability distributions along with Monte Carlo methods to generate a collection of points on or near a variety via an entirely different mechanism.

The basic approach proposed in this article is composed of two parts: first, constructing probability distributions that concentrate their mass near the variety of interest; and second, sampling from those distributions. Depending on the application of interest, if points actually on the variety are desired, endgames from numerical algebraic geometry can be applied to move the points to the variety reliably. For the probability distributions we propose new families of multivariate distributions called variety distributions. We describe these in Sections 2 and 3, which also provide a framework for semi-algebraic sets. The variety normal distributions introduced Section 2 form distinguished families of such distributions that appear particularly useful in applications. To sample from the distributions, we use Hamiltonian Monte Carlo (HMC), a Markov chain Monte Carlo (MCMC) variant currently at the forefront of Bayesian computing and well suited for these kinds of algebraic problems. This is presented in Section 4 along with a trick that allows the variety normal distribution to be expressed as a posterior distribution of a Bayesian analysis. Among other things, this enables the use of high quality software from the Bayesian statistics community to do the sampling efficiently with very little effort. In Section 5, we showcase a few applications of the method. We conclude in Section 6 with a discussion on the proposed method and future directions.

## 2 Variety normal distributions

In this section we construct a family of probability distributions that focus their mass on a variety of interest based on the normal and multivariate normal distributions. We begin with an observation about the univariate normal distribution that is later generalized greatly.

### 2.1 The variety normal distribution of a single polynomial

The univariate normal distribution is characterized by a probability density function (PDF) with respect to the Lebesgue measure on  $\mathbb{R}$  of the form  $p(x|\mu, \sigma^2) = \frac{1}{\sqrt{2\pi}\sigma} \exp\{-\frac{1}{2\sigma^2}(x - \mu)^2\}$ , where  $\mu \in \mathbb{R}$  and  $\sigma^2 > 0$  are given quantities. Disregarding normalization factors, the normal density is proportional to the exponential of a negative quadratic form, written  $p(x|\mu, \sigma^2) \propto \exp\{-\frac{1}{2\sigma^2}(x - \mu)^2\}$  or  $\tilde{p}(x|\mu, \sigma^2) = \exp\{-\frac{1}{2\sigma^2}(x - \mu)^2\}$ , where the tilde is used to express an un-normalized density, which we sometimes refer to as a pseudodensity.

The normal distribution focuses its mass on  $\mu$ , not merely in the sense that if  $X \sim p(x|\mu, \sigma^2)$  the expected value  $\mathbb{E}[X] = \mu$ , but also and perhaps more fundamentally in the sense that the mode of the distribution of

---

<sup>1</sup>As an important exception, it should be noted that many statistical models can be seen to be varieties whose corresponding ideals have Gröbner bases that can be determined combinatorially. [Drton et al., 2008]

$X$  is  $\mu$  and the density exponentially and symmetrically decays as one moves away from  $\mu$ . The dispersion parameter  $\sigma^2$ , the variance of  $X$ , describes the extent to which the distribution is concentrated on  $\mu$ : the closer to 0  $\sigma^2$  is, the more focused the distribution is on  $\mu$ . Importantly, the normal distribution focuses its mass where the quantity in the exponent vanishes. In the case of the univariate normal, this is the root of the linear polynomial  $g = x - \mu \in \mathbb{R}[x]$ . The variety is zero-dimensional:  $\mathcal{V}(g) = \{\mu\}$ .

We note in passing that the  $\frac{1}{2}$  can be absorbed into the polynomial  $p(x|\mu, \sigma^2) \propto \exp\{-\frac{1}{\sigma^2}(\frac{1}{\sqrt{2}}x - \frac{1}{\sqrt{2}}\mu)^2\}$  so that the coefficient vector of the polynomial lies on the unit sphere (here circle). This might have some benefit in providing a canonical representation of the polynomial; however, as we are not here interested in the parameter space but rather the individual distribution itself given  $g$ , and since the representation using the standard normal density has benefits later on, we leave the description as-is.

The observation that the normal distribution concentrates its mass near the variety of the linear polynomial  $g = x - \mu \in \mathbb{R}[x]$  suggests that the same is true for an arbitrary multivariate polynomial  $g(\mathbf{x}|\boldsymbol{\beta}) \in \mathbb{R}[\mathbf{x}]$ : if one wishes to construct a distribution that places its mass near  $\mathcal{V}(g)$ , simply swap  $x - \mu$  for  $g$ . This brings us to the heteroskedastic variety normal distribution.

**Definition 1.** A random vector  $\mathbf{X} \in \mathbb{R}^n$  is said to have the heteroskedastic variety normal (HVN) distribution, denoted  $\mathbf{X} \sim \mathfrak{N}_n(g, \sigma^2)$ , if it admits a density

$$p(\mathbf{x}|g, \sigma^2) \propto \tilde{p}(\mathbf{x}|g, \sigma^2) := \exp\left\{-\frac{g(\mathbf{x}|\boldsymbol{\beta})^2}{2\sigma^2}\right\} \quad (1)$$

with respect to the Lebesgue measure on  $\mathbb{R}^n$  for some  $g(\mathbf{x}|\boldsymbol{\beta}) \in \mathbb{R}[\mathbf{x}]$  and  $\sigma^2 > 0$ .  $\mathbf{X}$  is said to have the truncated HVN distribution, denoted  $\mathbf{X} \sim \mathfrak{N}_{n,\mathcal{X}}(g, \sigma^2)$ , if (1) only holds on some non-null  $\mathcal{X} \subset \mathbb{R}^n$ , outside of which  $p$  vanishes.

The conditional notation  $|g$ , indicating  $g$  is given, is unconventional since it incorporates both the coefficients of the polynomial  $\boldsymbol{\beta}$ , which are parameters, and the variates  $\mathbf{x}$  themselves. Nevertheless, for the present purposes  $|g$  comports a clarity that the vector of coefficients does not, so we find it to be a useful device to communicate intent.

Just as the univariate normal distribution focuses its mass on  $\mu$ , the HVN focuses its mass on the variety  $\mathcal{V}(g)$ : the  $-g^2$  in the exponent demands that the pseudodensity is maximized at the variety (if nonempty) and from there decreases (locally at least) so that the variety is the mode of the distribution. Indeed, the HVN can be thought of as a blurred version of a variety, where  $\sigma^2$  governs the amount of blurring. Probabilistically,  $\sigma^2$  is intended to gauge the likelihood of points falling a given distance away from the variety. In the simple univariate normal case, the variety is linear and zero-dimensional, and the empirical rule helps us interpret  $\sigma = \sqrt[3]{\sigma^2}$ . The general case is more complex. An example of the bivariate nonlinear case is illustrated in Figure 1 with  $g = x^2 + y^2 - 1 \in \mathbb{R}[x, y]$ . Figure 1 suggests the scheme works perfectly; however, a few considerations meter this enthusiasm: normalizability and the role of  $\sigma^2$ . We start with the role of  $\sigma^2$  and defer the discussion concerning normalizability to Section 2.3.

Coming from the normal distribution, it feels natural to want to interpret  $\sigma^2$  as gauging the amount of variability uniformly across the variety in the sense any two points in  $\mathbb{R}^n$  the same distance away from the variety should have the same likelihood of occurring, at least approximately. By distance here we simply mean the Euclidean distance from the points to the nearest point on the variety. (These closest points may not be unique, of course.) Unfortunately, however, the HVN distribution does not obey this basic intuition, as is easily seen with the polynomial  $g = y^2 - (x^3 + x^2) \in \mathbb{R}[x, y]$ , whose variety is the alpha curve displayed in red in Figure 2. This explains the adjective heteroskedastic, which does not here refer to variability changing on account of another variable per se but across the variety itself. It is the phenomenon where two points, similarly situated with respect to the variety, can have quite different likelihoods of occurring.

Why does this happen? Recalling that varieties are zero level sets, the HVN distribution can be thought of as shifting the graph of  $g$ , a surface in  $\mathbb{R}^3$ , up or down by a random amount following a  $\mathcal{N}(0, \sigma^2)$  distribution and selecting a point on the resulting zero level set. However, the shifting has varying effects across the variety: equal amounts of shifting do not result in equal amounts of movement of the zero level set across the intersection with the  $\mathbf{x}$ -plane. Figure 2 illustrates this with five equally spaced level sets of  $g$ .



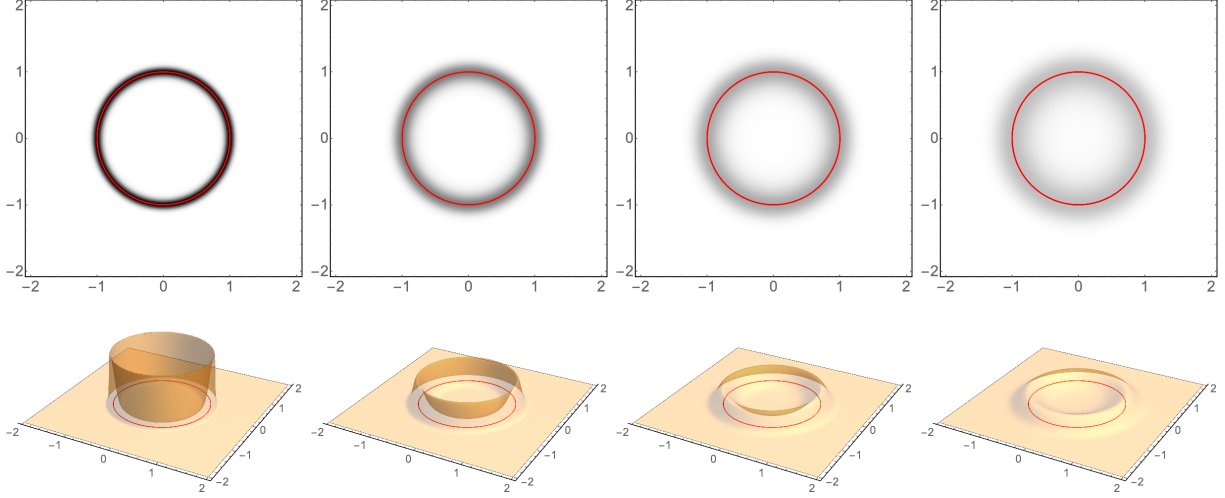


Figure 1: (Left to right.)  $\mathfrak{N}_2(x^2 + y^2 - 1, \sigma^2)$  from (1) with  $\sigma = .1, .2, .3$ , and  $.4$ ;  $\mathcal{V}(g)$  in red.

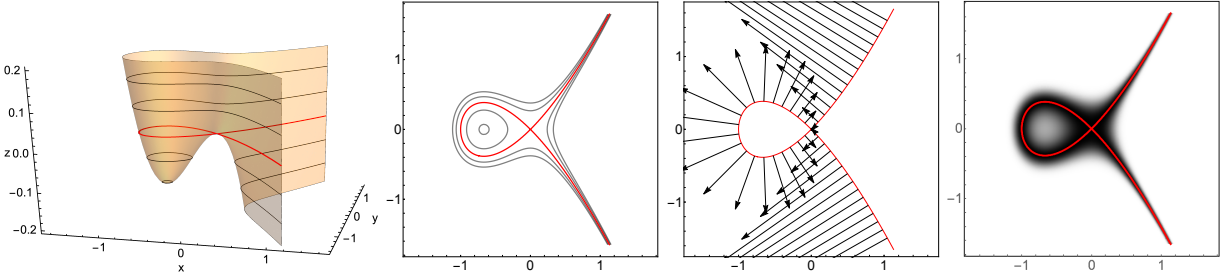


Figure 2: Equidistant level sets of  $g = y^2 - (x^3 + x^2)$  do not result equidistant contours. From left to right: The graph of  $g$  with equally spaced slices in  $z$ ; those intersections projected down into the  $xy$ -plane; the gradient vector field on the variety; and the density plot of the HVN with  $\sigma = .1$ .

This is in fact a general feature of level sets related to the inverse function theorem: parts of the variety where the function changes rapidly exhibit small changes, and places where it changes gradually exhibit large changes. This basic phenomenon is easily seen in univariate linear and quadratic polynomials; see Figure 3. In one dimension, for a nonconstant univariate linear polynomial  $g = \beta_0 + \beta_1 x \in \mathbb{R}[x]$ ,  $\mathcal{V}(g) = \{-\beta_0/\beta_1\}$ . Shifting the graph of  $g$  up by  $\epsilon$  moves the root from  $-\beta_0/\beta_1$  to  $-\beta_0/\beta_1 - \epsilon/\beta_1$ , i.e. an amount proportional to  $\beta_1^{-1}$  and in the direction of the opposite of the sign of  $\beta_1$ . Shifting it down by  $\epsilon$  moves it the same amount, but in the other direction—the direction of the sign of  $\beta_1$ , the derivative/slope of  $g$ .

In general, root mobility is inversely related to the magnitude of the gradient and in the opposite direction if the shift is up  $(+\epsilon)$  or the same direction if the shift is down  $(-\epsilon)$ . This is because the gradient  $\nabla_{\mathbf{x}} g$  points in the direction of steepest ascent, so near the variety (where  $g$  is 0) shifting the graph up requires a negative offset (a decrease from 0) to balance to 0, and this occurs in the direction of the negative gradient, assuming simple roots of course. Similarly, shifting the graph down moves the root in the direction of the gradient, the direction that would be required to move the value of the function  $g$  from 0 to a sufficiently positive value to offset the shift down. Curvature of the graph, a departure from linearity, affects an asymmetry in the magnitude of root mobility in same-sized upward and downward shifts, but this asymmetry is negligible for sufficiently small shifts up and down. In the current setting, this phenomenon can be observed at different points on the same variety, e.g. the images of Figure 2. The varying amount of change in the gradient's

magnitude results in a disproportionate amount of the distribution's mass being placed on areas where the surface near the variety is relatively flat.

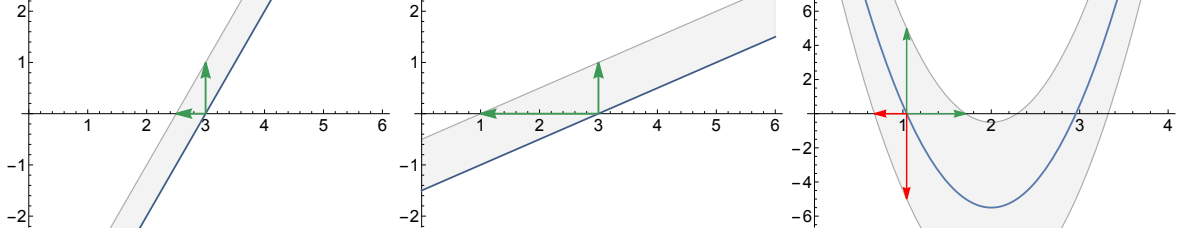


Figure 3: For a fixed amount of shifting up/down, varieties of rapidly changing functions exhibit less change than those of slowly changing functions. Curvature modulates this change in different directions.

The chief problem with the HVN distribution is that because  $g(\mathbf{x}|\boldsymbol{\beta})$  changes at different rates across the variety, the volume traversed in the ambient space  $\mathbb{R}^n$  by the surface as it is shifted up and down is uneven across the variety, and so the HVN distribution does not faithfully represent the notion that  $\sigma^2$  gauges proximity to the variety in a constant way across the whole of the variety. Depending on the context and use case, this may be considered a feature of the HVN; however, for our purposes we consider it a defect.

One solution to this problem is to locally linearize the surface to a constant scale by normalizing  $g$  by the size of its gradient; that is, to use  $\bar{g} = \bar{g}(\mathbf{x}|\boldsymbol{\beta}) = \frac{g}{\|\nabla_{\mathbf{x}} g\|}$  instead of  $g$  in place of the linear form  $\mathbf{x} - \boldsymbol{\mu}$  in the normal density. (Norms this article are assumed to be the 2-norm.) This can be justified by expanding  $g$  in a Taylor series about a point  $\mathbf{x} \in \mathcal{V}(g) \subset \mathbb{R}^n$ . Since  $g(\mathbf{x}) = 0$ ,

$$g(\mathbf{x} + \mathbf{h}) = \nabla g(\mathbf{x})' \mathbf{h} + o(\|\mathbf{h}\|) = \|\nabla g(\mathbf{x})\| \|\mathbf{h}\| \cos \theta + o(\|\mathbf{h}\|),$$

where  $\theta$  is the angle between the gradient  $\nabla g(\mathbf{x})$  and  $\mathbf{h}$ . Dividing by the norm of the gradient provides

$$\frac{g(\mathbf{x} + \mathbf{h})}{\|\nabla g(\mathbf{x})\|} = \|\mathbf{h}\| \cos \theta + o(\|\mathbf{h}\|),$$

where the  $o$  term is unaffected since  $\|\nabla g(\mathbf{x})\|$  is a constant with respect to  $\mathbf{h}$ . This of course assumes the gradient is nonzero. Note two facts: 1) where  $\|\nabla g\| \neq 0$ , the zero locus of  $\bar{g}$  is precisely that of  $g$ , and 2)  $\|\nabla g\| = 0$  on a set of Lebesgue measure 0, since  $\|\nabla_{\mathbf{x}} g\| = 0 \iff \|\nabla_{\mathbf{x}} g\|^2 = 0$ , and the latter only occurs on a set of measure 0 because  $\|\nabla_{\mathbf{x}} g\|^2$  is polynomial.<sup>2</sup> As PDFs are only defined up to equivalence classes that allow for modifications on sets of measure zero, the un-normalized density that uses the normalized expression  $\bar{g}$  is, up to normalizability at least, properly defined. Analogues to Figure 2 using the normalized version of  $g$  are presented in Figure 4.

With these things in mind, we are now able to present the definition we adopt in this work as the variety normal distribution.

**Definition 2.** A random vector  $\mathbf{X} \in \mathbb{R}^n$  is said to have the (homoskedastic) variety normal (VN) distribution, denoted  $\mathbf{X} \sim \mathcal{N}_n(g, \sigma^2)$ , if it admits a density

$$p(\mathbf{x}|g, \sigma^2) \propto \tilde{p}(\mathbf{x}|g, \sigma^2) := \exp \left\{ -\frac{\bar{g}(\mathbf{x}|\boldsymbol{\beta})^2}{2\sigma^2} \right\} = \exp \left\{ -\frac{1}{2\sigma^2} \left( \frac{g(\mathbf{x}|\boldsymbol{\beta})}{\|\nabla_{\mathbf{x}} g(\mathbf{x}|\boldsymbol{\beta})\|} \right)^2 \right\} \quad (2)$$

with respect to the Lebesgue measure on  $\mathbb{R}^n$  for some  $g(\mathbf{x}|\boldsymbol{\beta}) \in \mathbb{R}[\mathbf{x}]$  such that  $\bar{g}(\mathbf{x}|\boldsymbol{\beta}) = \frac{g(\mathbf{x}|\boldsymbol{\beta})}{\|\nabla_{\mathbf{x}} g(\mathbf{x}|\boldsymbol{\beta})\|}$  and  $\sigma^2 > 0$ .  $\mathbf{X}$  is said to have the truncated (homoskedastic) variety normal distribution, denoted  $\mathbf{X} \sim \mathcal{N}_{n,\mathcal{X}}(g, \sigma^2)$ , if (2) only holds on some non-null  $\mathcal{X} \subset \mathbb{R}^n$ , outside of which  $p$  vanishes.

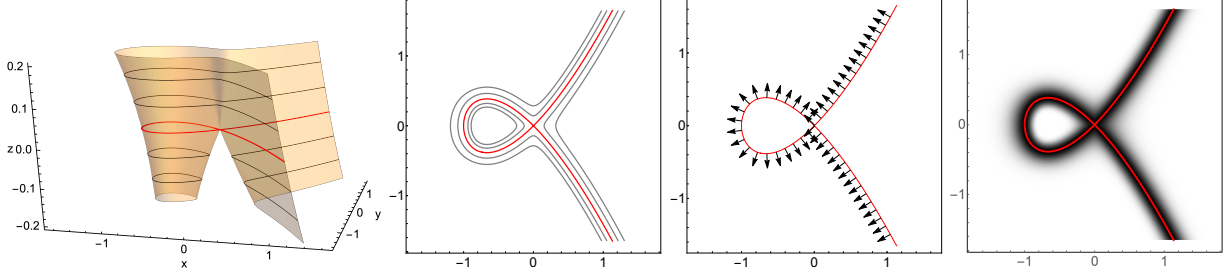


Figure 4: Equidistant level sets of  $\bar{g} = g / \|\nabla_{\mathbf{x}} g\|$  result in approximately equidistant contours ( $\sigma = .1$ ). Vectors drawn with  $2\sigma$  magnitude.

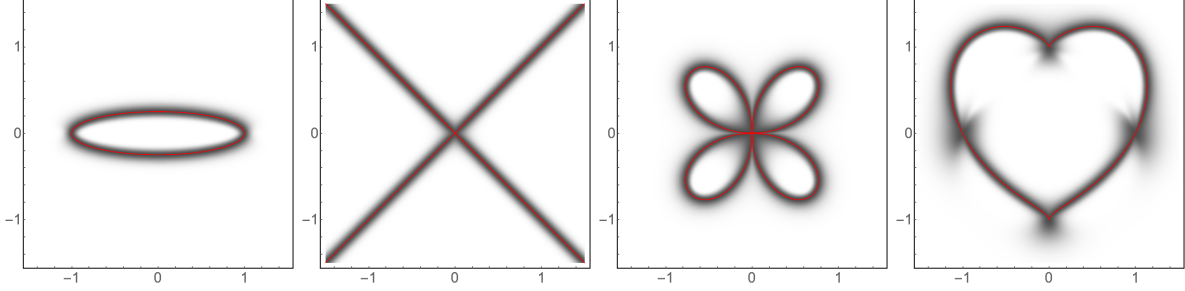


Figure 5: From left to right, density plots of  $\mathcal{N}_{2,\mathbf{x}}(\bar{g}, \sigma^2)$ , truncated to the window, with  $g = x^2 + (4y)^2 - 1$ ,  $(y - x)(y + x)$ ,  $(x^2 + y^2)^3 - 4x^2y^2$ , and  $(x^2 + y^2 - 1)^3 - x^2y^3$  and  $\sigma = .05$ . Aesthetic scales are consistent across the images. Note abnormalities at singularities in the last image.

We present density plots for several bivariate variety normal distributions in Figure 5.

Of course, the VN distribution is not only defined for distributions on  $\mathbb{R}^2$ , but any dimensional real space; the distributions just become more difficult to view. In  $\mathbb{R}^3$  the Whitney umbrella given by  $g(x, y, z) = x^2 - y^2z$  is illustrative of the general character of these distributions. Figure 6 provides 3D density visuals of this distribution with different amounts of variability; as the Whitney umbrella is not compact, a truncation is used.

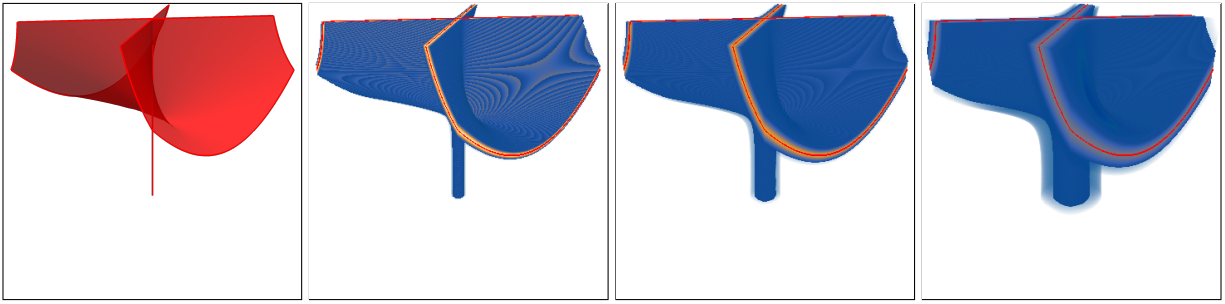


Figure 6: (Left) The Whitney umbrella defined by  $g(x, y, z) = x^2 - y^2z$  is the union of a one-dimensional handle and a two-dimensional canopy in  $\mathbb{R}^3$ . (Right) Three 3D density plots of the truncated VN distribution defined by the Whitney umbrella with  $\sigma = .025$ ,  $.05$ , and  $.10$ .

<sup>2</sup>And not the zero polynomial. In this article  $g$  is always nonconstant.

In light of this example, a helpful way to think of these distributions is as probabilistic thickenings of the variety into the ambient space  $\mathbb{R}^n$ . As the Whitney umbrella demonstrates, the thickening expands all components of the variety, regardless of dimension, into the full dimension of the ambient space. Moreover, the thickening is locally uniform across the variety in the sense that, away from singularities, two points equidistant from the variety have arbitrarily close probability density provided  $\sigma^2$  is selected sufficiently small. By construction, probability density decreases exponentially as one moves orthogonally away from the variety—in the direction parallel to the gradient. It is also approximately symmetric, with asymmetries arising from the curvature in  $g(\mathbf{x}|\boldsymbol{\beta})$  relative to the size of  $\sigma^2$ , the same effect as seen in Figure 3 (right). In Section 3 we describe how different kinds of thickenings can be performed.

## 2.2 The variety normal distribution as shifting surfaces

Before discussing normalizability and the multivariety normal distribution, we share a descriptive insight helpful in understanding the geometry of the VN distribution. The VN distribution admits an interesting interpretation as a four step procedure of selecting a random surface, intersecting it with a fixed surface, projecting the intersection, and randomly selecting a point in the resulting set. Let  $\pi : \mathbb{R}^{n+1} \rightarrow \mathbb{R}^n$  denote the coordinate projection  $(x_1, \dots, x_n, x_{n+1}) \mapsto (x_1, \dots, x_n)$  and  $\mathcal{G}_f = \{(\mathbf{x}, f(\mathbf{x})) : \mathbf{x} \in \mathbb{R}^n\} \subset \mathbb{R}^{n+1}$  the graph of the function  $f : \mathbb{R}^n \rightarrow \mathbb{R}$ , a  $n$ -dimensional hypersurface in  $\mathbb{R}^{n+1}$ . For  $c \in \mathbb{R}$ , let  $\mathcal{G}_c$  denote the flat  $n$ -dimensional hyperplane in  $\mathbb{R}^{n+1}$  at height  $c$  parallel to the  $\mathbf{x}$ -axis. Sampling the VN distribution then admits the following five perspectives, among others, each corresponding to different selections of hypersurfaces derived from manipulations of the equation  $\frac{g}{\|\nabla_{\mathbf{x}} g\|} - X = 0$  with  $X \sim \mathcal{N}(0, \sigma^2)$ . The first is the one that motivated our previous discussion.

- I.  $\mathcal{G}_{\bar{g}-X} \cap \mathcal{G}_0$ : randomly shift  $\mathcal{G}_{\bar{g}}$  up/down in  $\mathbb{R}^{n+1}$  by a  $\mathcal{N}(0, \sigma^2)$  draw, intersect it with the  $\mathbf{x}$ -axis, project the intersection onto the first  $n$  components, and sample uniformly from the resulting set.
- II.  $\mathcal{G}_{\bar{g}} \cap \mathcal{G}_X$ , randomly shift  $\mathcal{G}_0$  up/down in  $\mathbb{R}^{n+1}$  by a  $\mathcal{N}(0, \sigma^2)$  draw, intersect it with  $\mathcal{G}_{\bar{g}}$ , project the intersection onto the first  $n$  components, and sample uniformly from the resulting set.
- III.  $\mathcal{G}_g \cap \mathcal{G}_{X\|\nabla_{\mathbf{x}} g\|}$ , which has two interpretations:
  - (1) differentially scale the random flat plane  $\mathcal{G}_X$  by  $\|\nabla_{\mathbf{x}} g\|$ , intersect it with  $\mathcal{G}_g$ , project the intersection onto the first  $n$  components, and sample uniformly from the resulting set, or
  - (2) randomly scale  $\mathcal{G}_{\|\nabla_{\mathbf{x}} g\|}$  with a  $\mathcal{N}(0, \sigma^2)$  draw, intersect it with  $\mathcal{G}_g$ , project the intersection onto the first  $n$  components, and sample uniformly from the resulting set.
- IV.  $\mathcal{G}_{g-X\|\nabla_{\mathbf{x}} g\|} \cap \mathcal{G}_0$ : intersect a carefully selected random hypersurface in  $\mathbb{R}^{n+1}$  with the  $n$ -dimensional  $\mathbf{x}$ -axis, project the intersection onto the first  $n$  components, and sample uniformly from the resulting set.
- V.  $\mathcal{G}_{g^2-X^2\|\nabla_{\mathbf{x}} g\|^2} \cap \mathcal{G}_0$ , similar to the previous perspective but where the hypersurface is a variety, which is of interest as it is more algebraic. This approximates the offset variety [Horobet and Weinstein, 2018].

These perspectives are illustrated in Figure 7.

## 2.3 Normalizability, emptiness, and near roots

## 2.4 The multivariety normal distribution

It is natural at this point to consider the relationship between the VN distribution and the multivariate normal distribution: both are multivariate distributions and both generalize the univariate normal distribution. One key difference is that, like the univariate normal distribution, the multivariate normal distribution always concentrates its mass around a single point, the zero-dimensional variety  $\mathcal{V}(\mathbf{x} - \boldsymbol{\mu}) = \{\boldsymbol{\mu}\}$ , whereas the VN distribution can support a positive-dimensional variety. A second difference can be found in the variability

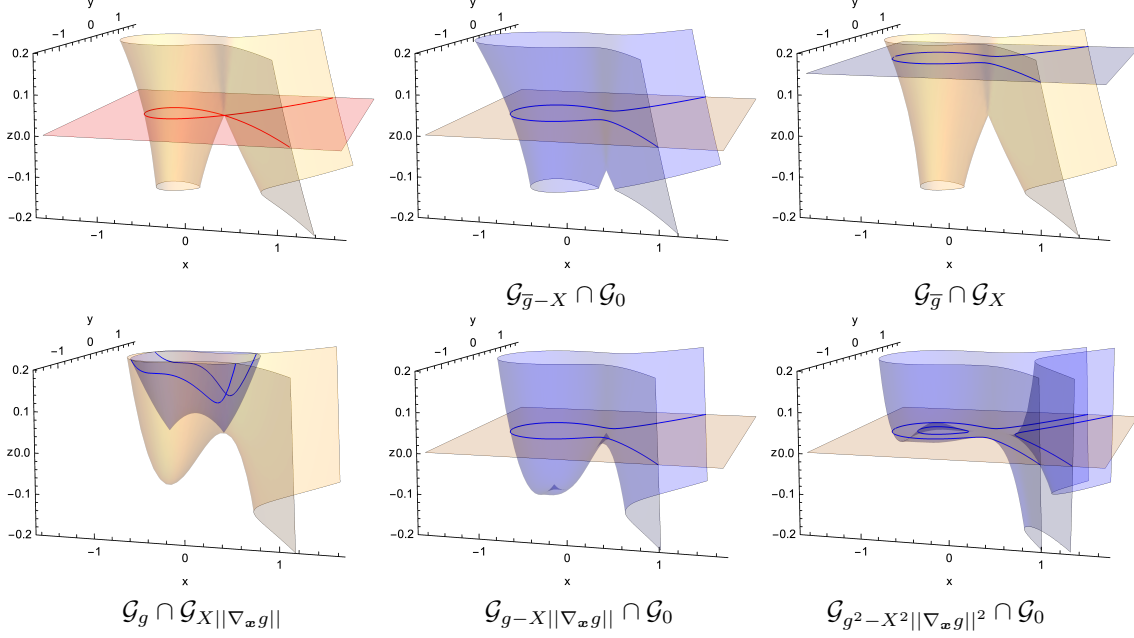


Figure 7: Geometrically, the variety normal distribution can be seen from various perspectives as selecting a point at the intersection of a fixed and a random surface (projected into  $\mathbb{R}^n$ ). Perspectives I–V. are illustrated, with the random surface in blue. In each case, the random surface illustrated was generated with  $X = .15$ , i.e. at 1.5 “standard deviations” from the variety with  $\sigma = .1$ .

about the variety: in the VN distribution,  $\sigma^2$  gauges deviations from the variety globally and isotropically, whereas the multivariate normal distribution can support differing amounts of variability anisotropically. In fact, the VN distribution can be generalized to support this kind of variability as well. This leads us to a more general formulation of the VN distribution.

**Definition 3.** A random vector  $\mathbf{X} \in \mathbb{R}^n$  is said to have the multivariety normal (MVN) distribution, or simply the variety normal distribution, denoted  $\mathbf{X} \sim \mathcal{N}_n(\mathbf{g}, \mathbf{\Sigma})$ , if it admits a density

$$p(\mathbf{x}|\mathbf{g}, \mathbf{\Sigma}) \propto \exp \left\{ -\frac{1}{2} \bar{\mathbf{g}}(\mathbf{x}|\mathbf{B})' \mathbf{\Sigma}^{-1} \bar{\mathbf{g}}(\mathbf{x}|\mathbf{B}) \right\} \quad (3)$$

$$= \exp \left\{ -\frac{1}{2} (\mathbf{J}_x^+ \mathbf{g}(\mathbf{x}|\mathbf{B}))' \mathbf{\Sigma}^{-1} (\mathbf{J}_x^+ \mathbf{g}(\mathbf{x}|\mathbf{B})) \right\} \quad (4)$$

with respect to the Lebesgue measure on  $\mathbb{R}^n$  for some  $\mathbf{g}(\mathbf{x}|\mathbf{B}) \in \mathbb{R}[\mathbf{x}]^m$  such that  $\bar{\mathbf{g}}(\mathbf{x}|\mathbf{B}) = \mathbf{J}_x^+ \mathbf{g}(\mathbf{x}|\mathbf{B})$ , where  $\mathbf{J}_x^+$  is the  $n \times m$  pseudoinverse of the  $m \times n$   $\mathbf{x}$ -Jacobian matrix of  $\mathbf{g}(\mathbf{x}|\mathbf{B})$ , and  $\mathbf{\Sigma} \in \mathbb{S}_+^n$ , the cone of symmetric positive definite  $n \times n$  matrices.

$\bar{\mathbf{g}}(\mathbf{x}|\mathbf{B}) = \mathbf{J}_x^+ \mathbf{g}(\mathbf{x}|\mathbf{B})$  generalizes the notion of normalizing by the gradient. Considering  $\mathbf{g}$  as the vector field  $\mathbf{g} : \mathbb{R}^n \rightarrow \mathbb{R}^m$ , the local linear approximation to points on the variety (properly translated) is given by  $\mathbf{J}_x \in \mathbb{R}^{m \times n}$ , which is “inverted” by  $\mathbf{J}_x^+ \in \mathbb{R}^{n \times m}$ . In the square case, at smooth points the inverse function theorem guarantees that  $\bar{\mathbf{g}}(\mathbf{x}|\mathbf{B})$  will be properly normalized so that  $\mathbf{\Sigma}$  gauges “covariance” globally across  $\mathcal{V}(\mathbf{g})$ . Several such square MVN distributions over zero-dimensional varieties are illustrated in Figure 8. If there are more variables than equations ( $n > m$ ), the Jacobian represents an underdetermined system corresponding to a positive dimensional variety;  $\mathbf{J}_x$  is full row rank for almost all  $\mathbf{x} \in \mathbb{R}^n$ , and  $\mathbf{J}_x^+ = \mathbf{J}_x' (\mathbf{J}_x \mathbf{J}_x')^{-1}$ . Previous examples of the variety normal, a single equation in many variables, are in fact examples of this situation. If there are more equations than variables ( $m > n$ ) but the variety is nonempty, the Jacobian represents an

overdetermined system;  $\mathbf{J}_x$  is full rank for almost every  $\mathbf{x} \in \mathbb{R}^n$ ; and  $\mathbf{J}_x^+ = (\mathbf{J}_x' \mathbf{J}_x)^{-1} \mathbf{J}_x'$ . Either way,  $\mathbf{J}_x^+$  transforms the original  $m$ -dimensional  $\mathbf{g}$  into an  $n$ -dimensional vector  $\bar{\mathbf{g}}$  compatible with  $\Sigma$ .

As one might expect, the multivariety normal family of distributions subsumes the variety normal and multivariate normal families. And, since the multivariety normal subsumes the multivariate normal, it subsumes the matrix-variate normal and tensor-variate normal (also called the multilinear normal) families as well [Ohlson et al., 2013]. We now explain how this works.

If  $m = 1$  and  $\Sigma = \sigma^2 \mathbf{I}_n$ , the multivariety normal distribution reduces to the variety normal distribution. To see this, define  $\mathbf{d} = \nabla_{\mathbf{x}} g(\mathbf{x}|\beta)$  and note that in the  $m = 1$  case  $\mathbf{g}(\mathbf{x}|\beta) = g(\mathbf{x}|\beta) = g$ ,  $\mathbf{J}_x = \mathbf{d}'$ , and  $\mathbf{J}_x^+ = \mathbf{d}(\mathbf{d}'\mathbf{d})^{-1} = \frac{1}{\|\mathbf{d}\|^2} \mathbf{d}$ . So if  $\Sigma = \sigma^2 \mathbf{I}_n$ ,

$$\begin{aligned} \exp \left\{ -\frac{1}{2} (\mathbf{J}_x^+ \mathbf{g})' \Sigma^{-1} (\mathbf{J}_x^+ \mathbf{g}) \right\} &= \exp \left\{ -\frac{1}{2} \left( \left( \frac{1}{\|\mathbf{d}\|^2} \mathbf{d} \right) g \right)' (\sigma^2 \mathbf{I}_n)^{-1} \left( \left( \frac{1}{\|\mathbf{d}\|^2} \mathbf{d} \right) g \right) \right\} \\ &= \exp \left\{ -\frac{1}{2\sigma^2} \left( \frac{g}{\|\mathbf{d}\|} \left( \frac{\mathbf{d}}{\|\mathbf{d}\|} \right)' \left( \frac{\mathbf{d}}{\|\mathbf{d}\|} \right) \frac{g}{\|\mathbf{d}\|} \right) \right\} \\ &= \exp \left\{ -\frac{1}{2\sigma^2} \left( \frac{g}{\|\nabla_{\mathbf{x}} g\|} \right)^2 \right\} = \exp \left\{ -\frac{\bar{g}^2}{2\sigma^2} \right\}, \end{aligned}$$

which is (2), the PDF of the variety normal distribution. More generally, if the system is not overdetermined,  $\mathbf{J}_x$  typically has  $m$  independent rows and so if  $\Sigma = \sigma^2 \mathbf{I}_n$ ,

$$p(\mathbf{x}|\mathbf{g}, \Sigma) \propto \exp \left\{ -\frac{1}{2\sigma^2} \mathbf{g}' (\mathbf{J}_x \mathbf{J}_x')^{-1} \mathbf{g} \right\}. \quad (5)$$

If  $\mathbf{g} = \mathbf{x} - \boldsymbol{\mu}$ ,  $m = n$  and  $\mathbf{J}_x = \mathbf{I}_n$ , and the distribution reduces to the multivariate normal. The individual varieties of the  $g_i$ 's are the  $n$  hyperplanes of dimension  $n - 1$  that run parallel to the coordinate axes and intersect at the point  $\boldsymbol{\mu}$ .

An added nuance of the MVN distribution not present in the VN distribution is that of covariance, or rather what would be covariance in a multivariate normal distribution. The covariance for MVN distributions is far more complex than the parameters themselves and not of primary interest, like other moments for variety normal distributions. Figure 9 considers the variety corresponding to the polynomial  $g = x^2 + y^2 - 1$  using  $\Sigma = \begin{bmatrix} \sigma_1 & 0 \\ 0 & \sigma_2 \end{bmatrix} \begin{bmatrix} 1 & \rho \\ \rho & 1 \end{bmatrix} \begin{bmatrix} \sigma_1 & 0 \\ 0 & \sigma_2 \end{bmatrix}$  with  $\sigma_1 = \sigma_2 = .2$  and  $\rho = 0, .9$ , and  $-.9$ . When  $\rho = 0$ , the variability about  $\mathcal{V}(\mathbf{g})$  is isotropic; this is the ‘‘independence’’ case. When it is positive, variability is oriented towards regions of same-signed coordinates, and the opposite when it is negative. Figure 10, the one dimensional variety generated by the two polynomials  $g_1 = x^2 + y^2 - 1$  and  $g_2 = z$ , illustrates the effect of ‘‘correlation’’ among the three variables, which can be very complex.

Understanding a variety tends to be easiest when correlations are zero, so that  $\Sigma$  is diagonal, and the magnitude of the thickening (variability) in each coordinate axis is uniform, so that  $\Sigma = \sigma^2 \mathbf{I}_n$ . In principle, the smaller the  $\sigma^2$ , the better; however, if  $\sigma^2$  is chosen to be too small, the sampling schemes described in Section 4 tend to not perform as well. We revisit this topic there and in Section 5.2.

### 3 Induced variety distributions

The construction of the variety normal distributions admits a different interpretation that leads to a nice generalization whereby one can put essentially any distribution around a variety in the same way that those distributions put a normal around it. In the VN case, instead of thinking of  $\bar{g}(\mathbf{x}|\beta)$  as replacing  $\mathbf{x} - \boldsymbol{\mu}$  in the normal kernel, one can think of taking any distribution in the normal family, applying a location transformation so that the mode is zero, and then substituting  $\bar{g}(\mathbf{x}|\beta)$  for  $\mathbf{x}$ ; it just so happens that in the normal case this location transformation resets  $\boldsymbol{\mu}$  to 0. The same is true for the MVN case by replacing  $\mathbf{x} - \boldsymbol{\mu}$  with  $\bar{g}(\mathbf{x}|\mathbf{B})$ . This same process applies generally:



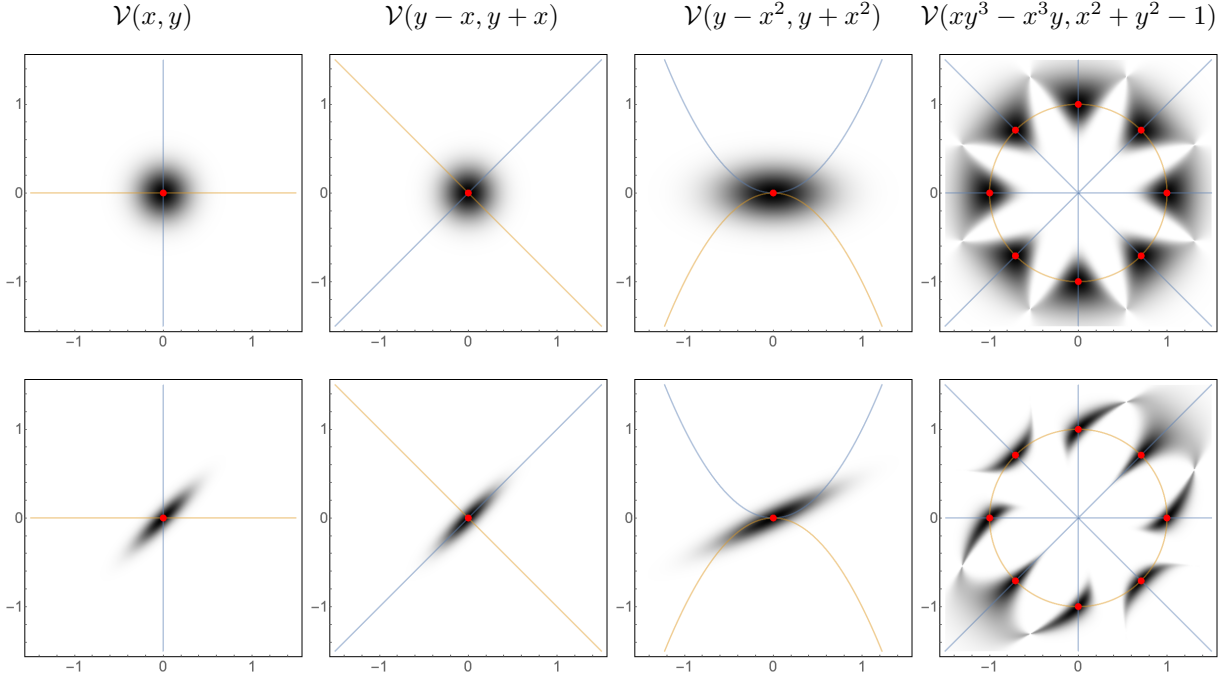


Figure 8: Multivariety normal distributions over zero-dimensional varieties and their associated systems with no “correlation” (top) and positive “correlation” ( $\rho = .9$ , bottom). In each case  $\Sigma = \sigma^2 \mathbf{I}$ . While  $\sigma^2 = .2^2$  in each case, the density color scales and  $z$ -axes ranges vary across graphics.

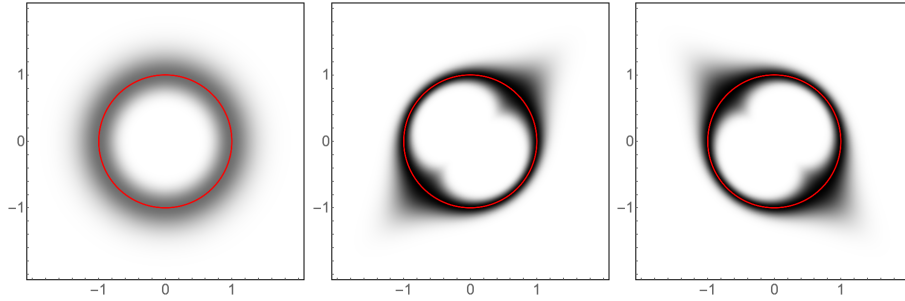


Figure 9: Multivariety normal densities with  $g = x^2 + y^2 - 1$ ,  $\sigma_1 = \sigma_2 = .2$ , and  $\rho = 0, .9, -.9$ .

1. Select a univariate or multivariate distribution with features of interest, e.g. unimodality,
2. Shift the distribution’s location to the origin, rescaling as desired, and
3. Substitute  $\bar{g}(\mathbf{x}|\mathbf{B})$  for  $\mathbf{x}$  in the resulting expression.

We refer to these distributions as induced variety distributions.

It is helpful to illustrate the process on a univariate family. Suppose again we are interested in the alpha curve, the variety of  $g = y^2 - (x^3 - x^2)$ , but want to use a uniform distribution, a member of the beta family, instead of a normal. The PDF of the beta distribution is  $p(x|\alpha, \beta) \propto x^{\alpha-1}(1-x)^{\beta-1}$  on  $0 < x < 1$  for  $\alpha, \beta > 0$ ; the uniform occurs when  $\alpha = 1$  and  $\beta = 1$ . If  $X \sim p(x|\alpha, \beta)$ , it is a basic fact that if  $\sigma > 0$  and  $\mu \in \mathbb{R}$  the distribution of  $\sigma X + \mu$  is proportional to  $p(\frac{x-\mu}{\sigma}|\alpha, \beta)$  for  $x \in (\mu, \mu + \sigma)$ , so choosing  $\mu = -\frac{\sigma}{2}$  is

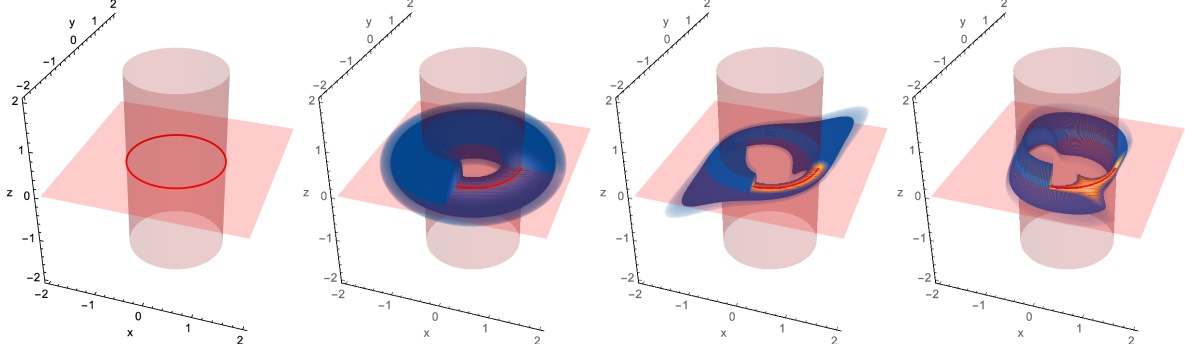


Figure 10: From left to right, the varieties of  $g_1 = x^2 + y^2 - 1$  and  $g_2 = z$  and their intersection  $\mathcal{V}(g_1, g_2)$ , the unit circle in the  $xy$  plane; and three 3D density plots of the MVN distribution with  $\sigma_1 = \sigma_2 = \sigma_3 = .2$  and  $\rho_{12} = \rho_{13} = \rho_{23} = 0$ ,  $\rho_{12} = \rho_{13} = \rho_{23} = .9$ , and  $\rho_{12} = -.9$ ,  $\rho_{13} = .5$ , and  $\rho_{23} = -.1$ . Aesthetic scales are consistent across graphics, and the  $x, z \geq 0, y \leq 0$  orthant has been removed to see inside the regions.

reasonable to center the distribution on zero. The resulting bivariate distribution described by the method is therefore  $p(x, y | \alpha, \beta, \mu, \sigma) \propto p(\frac{\bar{g} - \mu}{\sigma} | \alpha, \beta)$  with  $\bar{g} = (y^2 - (x^3 + x^2)) / \sqrt{(3x^2 + 2x)^2 + (2y)^2}$ . As  $\mathcal{V}(g)$  is not compact, we truncate the distribution to  $\mathcal{X} = [-1.5, 1.5]^2$ . This is illustrated in Figure 11 with  $\sigma = 1/2$  and various settings of  $\alpha$  and  $\beta$ . The asymmetry observed is an artifact of selecting  $\sigma$  too large relative to the linear approximation produced by the gradient normalization.

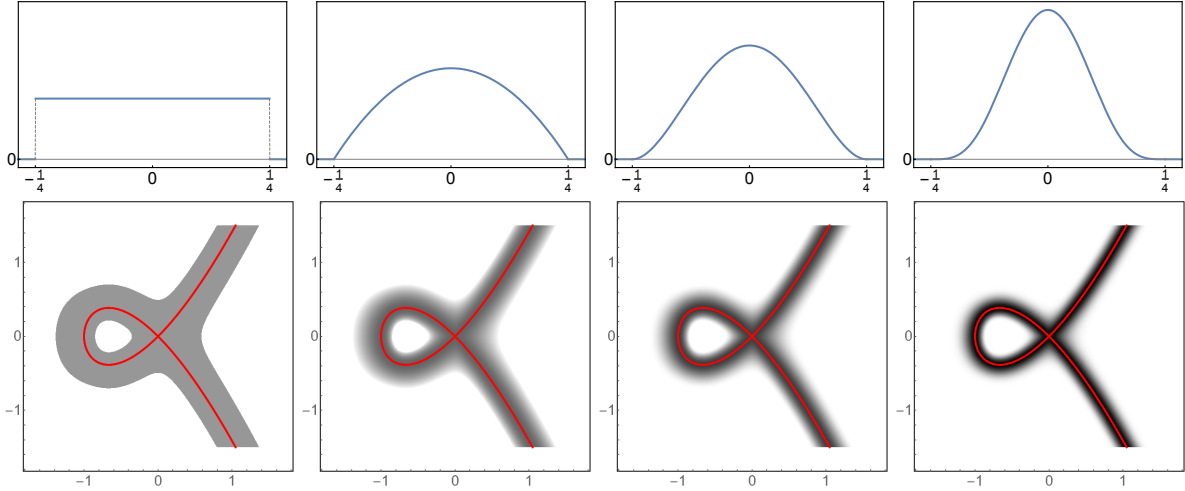


Figure 11: The induced variety beta distribution on the alpha curve with  $\sigma = 1/2$ ,  $\mu = -\sigma/2$ , and  $(\alpha, \beta) = (1, 1), (2, 2), (3, 3),$  and  $(5, 5)$ , from left to right.

While this strategy works, it doesn't seem to have many advantages over the variety normal distributions. One limitation is that if the selected distribution has compact support, the resulting distribution will not have the full support of  $\mathbb{R}^n$ , and consequently Hamiltonian samplers may be prone to more problems, e.g. initialization and feasible proposals. However, one observation about these distributions enables the creation of distributions about semi-algebraic sets.

### 3.1 Semi-algebraic distributions

Although the specific definition varies slightly, varieties are commonly referred to as algebraic sets in the literature. Semi-algebraic sets are generalizations of algebraic sets that allow for inequalities.

**Definition 4.** A semi-algebraic set is a set of the form  $\{\mathbf{x} \in \mathbb{R}^n : \mathbf{g}(\mathbf{x}) = \mathbf{0}_m \text{ and } \mathbf{h}(\mathbf{x}) > \mathbf{0}_l\}$  for  $\mathbf{g}(\mathbf{x}) \in \mathbb{R}[\mathbf{x}]^m$  and  $\mathbf{h}(\mathbf{x}) \in \mathbb{R}[\mathbf{x}]^l$ .

A few minor modifications to the strategies described above allow us to create distributions that focus their mass on semi-algebraic sets in the same way that variety distributions focus their mass on varieties. We note a quick trick at the outset, however, which is both common and useful in practice: if a single variable needs to be non-negative, it suffices to swap the variable with the square of another variable. As the square is always non-negative (over the reals), one simply retains the draws of the squared variable.

There are two basic approaches one can take to creating semi-algebraic distributions.

1. The first strategy is similar to the induced variety approach, but instead of picking a distribution that centers its mass on 0, pick a distribution that borders 0 by piling all its mass up against one side. We call the resulting distribution a border (induced variety) distribution. While this strategy seems like a good fit, it suffers from two drawbacks. First, while it works for varieties generated by a single polynomial, it is not clear how it could be conveniently applied to semi-algebraic sets in general, i.e. sets specified with several polynomials and a mix of equalities and inequalities. Second, the usefulness of the resulting distribution for understanding the semialgebraic set is very sensitive to the selection of the base distribution, often placing mass in the immediate vicinity of the boundary of the semi-algebraic set and almost entirely missing parts from from it.
2. The second strategy is to eliminate inequalities by converting them to equalities by introducing slack variables, placing a distribution about the corresponding variety in the higher dimensional space, and marginalizing out the slack variables. Geometrically, this corresponds to creating a variety in higher dimensional space whose projection is the semi-algebraic sets of interest. This strategy appears to largely alleviate both of the challenges faced by the first strategy.

As a simple illustration of these concepts, consider sampling from the unit disc  $\{(x, y) \in \mathbb{R}^2 : x^2 + y^2 < 1\}$ , which in canonical form is  $\{(x, y) \in \mathbb{R}^2 : h(x, y) > 0\}$  with  $h(x, y) = 1 - (x^2 + y^2)$ :

1. For a border distribution, we may select the uniform distribution as the base distribution:  $p(x|0, \beta) = 1[0 \leq x \leq \beta]$ . Following the approach of the previous section, no shifting of the distribution is required, since it comes up against 0 from above, and we can simply set the distribution of interest to be  $p(x, y|0, \beta) \propto 1[0 \leq \bar{h}(x, y) \leq 1]$ , where  $\bar{h}(x, y) = \frac{1 - (x^2 + y^2)}{2\sqrt{x^2 + y^2}}$ . This is illustrated in Figure 12.

Notice that the resulting distribution always exhibits a hole in the middle, resulting in a distribution on an annulus instead of the disk. While this is alleviated by forcing  $\beta$  to be large, it always induces the artificial hole. As an alternative, one may choose to use a base distribution without an upper bound such as the exponential distribution, whose density is  $p(x|\lambda) = \lambda e^{-\lambda x}$  for  $x \geq 0$ . This is illustrated in Figure 12. Unfortunately this, too, results in a noticeably non-uniform distribution. As a uniform distribution cannot be placed on all of  $\mathbb{R}_+$ , this strategy generally appears unsatisfying.

2. By contrast, the second strategy proceeds by recognizing that the condition  $h(x, y) > 0$  implies the existence of a positive number  $s^2$  such that  $g(x, y, s) = h(x, y) - s^2 = 0$ . Since this describes a variety in  $\mathbb{R}^3$ , we can use any of the methods of the previous sections to place a distribution on it. We can then marginalize out the lifting/slack/auxiliary variable  $s$  to obtain the distribution of interest. In this case, since  $g(x, y, s) = 1 - x^2 - y^2 - s^2$ , this corresponds to creating a distribution about the sphere in  $\mathbb{R}^3$  and marginalizing. This is illustrated in Figure 13.

For the reasons described above, the second strategy generally seems preferable to the first, and so we recommend it when presented with semi-algebraic sets. Nevertheless it, too, is imperfect, and more work is

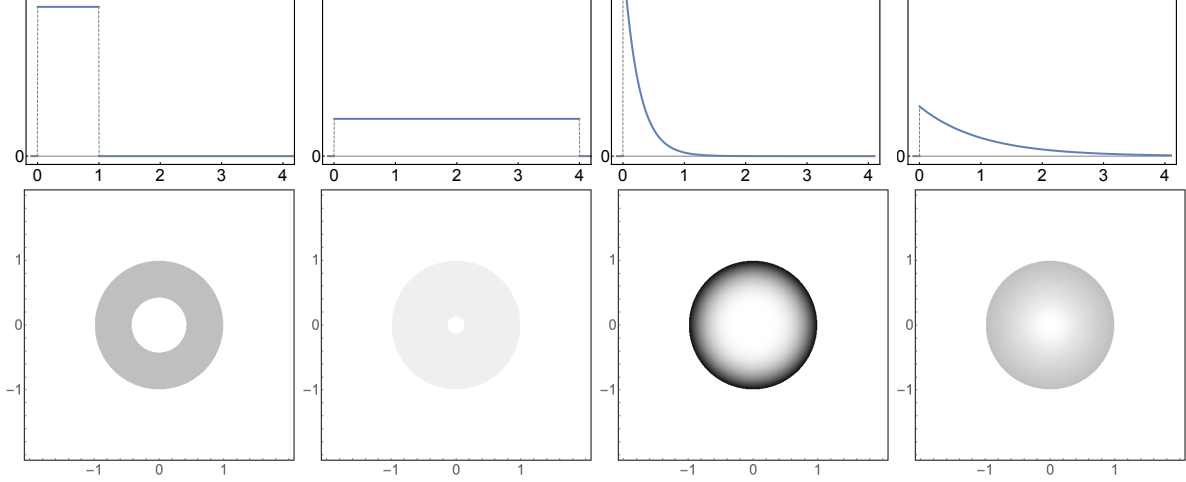


Figure 12: Distributions about semi-algebraic sets can be constructed by bordering distributions on one side of 0. From left to right, this is illustrated using the  $\text{Unif}(0, 1)$ ,  $\text{Unif}(0, 4)$ ,  $\text{Exp}(4)$ , and  $\text{Exp}(1)$  distributions.

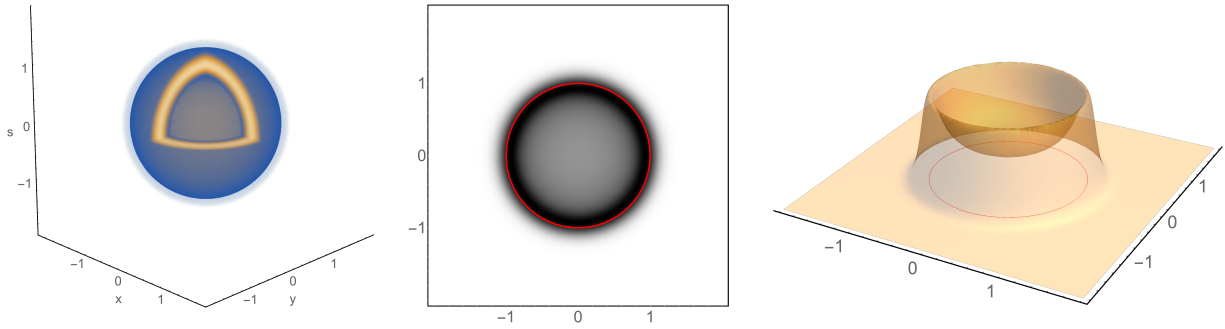


Figure 13: Distributions about semi-algebraic sets can be constructed as marginal distributions of variety distributions. (Left) A variety normal density on  $\mathcal{S}^2$  along with a cutaway to visualize variability. (Middle) A density plot of the margined distribution over the semi-algebraic set of the open unit disc. (Right) The graph of the joint PDF of the distribution of  $(X, Y)$ .

needed to develop a more satisfactory solution. Experimentally, the strategy presents some boundary effects where the distribution is slightly more concentrated near the boundary of the projected region; however, these appear to be relatively small in practice. It should also be noted that alternative algebraic formulations can be used to represent the semi-algebraic set of interest. For example, instead of moving from  $h(x, y) > 0$  to  $g(x, y, s) = h(x, y) - s^2 = 0$  in the above, we might have opted for  $g(x, y, s) = s^2 h(x, y) - 1 = 0$ . Unfortunately, the representation matters, and a bad representation may not work at all from a sampling perspective because the resulting varieties may be unbounded.

In general, if a semi-algebraic set is presented as above, it can be represented as the projection of the variety defined by  $g_1(\mathbf{x}), \dots, g_m(\mathbf{x}), h_1(\mathbf{x}) - s_1^2, \dots, h_l(\mathbf{x}) - s_l^2 \in \mathbb{R}[\mathbf{x}, \mathbf{s}]$  in  $\mathbb{R}^{p+l}$  [Bochnak et al., 1991, p.27]. In fact, Motzkin has shown that this can always be done by introducing only one slack variable [Motzkin, 1970, Bochnak et al., 1991]; however, as the current strategy is simple and effective, we saw no need to pursue it further. Pecker [1990] has found a similar yet simpler strategy.

It should be noted that semi-algebraic sets represent a very diverse collection of subsets of  $\mathbb{R}^p$ . In

particular, they can allow puncturing of sets and, more generally, the removal from larger dimensional sets smaller dimensional geometries. These cannot be faithfully represented by the present construction because variety distributions always thicken the variety into the fullness of the ambient space.

## 4 Sampling and the stochastic exploration of real varieties

In this section we describe practical strategies to sample from the distributions presented in the previous sections to generate points near the variety as well as methods to move those points to the variety. To ease the exposition and accentuate how nice the situation can be, we focus our presentation mainly on the variety normal distribution and note relevant differences for other induced variety distributions where key features stick out.

### 4.1 Sampling

There are many strategies one can use to sample from a probability distribution [Gentle, 2006, Robert and Casella, 2013]. For a given situation, the best sampler depends heavily on features of the distribution of interest, the target distribution. Perhaps most importantly from a sampling perspective, all the distributions described in this work are continuous on  $\mathbb{R}^n$  and only known up to an unknown constant of proportionality; this limits the strategies that can be used. Fortunately, there is already a wealth of knowledge on sampling from un-normalized distributions since these distributions form the foundation of Bayesian statistics. As such, Bayesian statisticians and others have developed very powerful general purpose tools to perform such sampling, both theoretically and in the form of freely accessible computer implementations. Before progressing to these more complex techniques, however, it is worth noting a simple one that works in many low-dimensional settings: rejection sampling.

#### 4.1.1 Rejection sampling

Rejection sampling relies on the following basic fact referred to by Robert and Casella [2013] as the Fundamental Theorem of Simulation (FTS): Given a (potentially un-normalized) PDF  $\tilde{p}(\mathbf{x})$ , sampling from  $\tilde{p}(\mathbf{x})$  is equivalent to sampling from the uniform distribution on the region below its graph,

$$\{(\mathbf{x}, u) \in \mathbb{R}^{n+1} : 0 \leq u \leq \tilde{p}(\mathbf{x})\}.$$

Rejection sampling refers to any algorithm that obtains such uniform draws by sampling uniformly from the region below a proposal distribution  $q(\mathbf{x})$  for which  $Mq(\mathbf{x}) \geq \tilde{p}(\mathbf{x})$  for some  $M \in \mathbb{R}$  and then checking if the draws are also under the graph of  $\tilde{p}(\mathbf{x})$ . Specifically: 1) sample  $\mathbf{x}' \sim q(\mathbf{x})$ , 2) sample  $u \sim \text{Unif}(0, Mq(\mathbf{x}'))$ , and 3) if  $u \leq \tilde{p}(\mathbf{x}')$ ,  $\mathbf{x}' \sim p(\mathbf{x})$  otherwise repeat the procedure. The resulting retained/accepted draws constitute an independent and identically distributed sample from  $p(\mathbf{x})$ , the normalized distribution corresponding to  $\tilde{p}(\mathbf{x})$ . The efficiency of the sampler depends on how similar  $q(\mathbf{x})$  is to  $p(\mathbf{x})$  and how small  $M$  is.

By construction, the un-normalized (multi)variety normal distributions' PDFs (2) and (3) are bounded above by 1, which is tight on the variety. If a spatial extent (range of the  $\mathbf{x}$  variables) is known a priori, one can therefore simply apply a rejection sampling algorithm over that extent using the uniform distribution.

As an example, consider sampling from the variety normal on the alpha curve,  $\mathcal{N}_{2,\mathcal{X}}(y^2 - (x^3 - x^2), \frac{1}{10^2})$  with  $\mathcal{X} = [-1.5, 1.5]^2$ , whose normalized polynomial was seen in the previous section to be  $\bar{g} = (y^2 - (x^3 + x^2))/\sqrt{(3x^2 + 2x)^2 + (2y)^2}$ . From (2), its un-normalized PDF is  $\tilde{p}(\mathbf{x}'|g, \sigma^2) = \exp\{-50\bar{g}^2\}$ . Thus, rejection sampling from the distribution would take two draws  $x, y \sim \text{Unif}(-1.5, 1.5)$  and one  $u \sim \text{Unif}(0, 1)$  and check if  $u \leq \tilde{p}(\mathbf{x}'|g, \sigma^2)$ . If so, we retain  $(x, y)$  as one draw from  $p(x, y|g, \sigma^2)$ , otherwise we repeat the procedure. This is illustrated in Figure 14.

Using this simple rejection scheme on the induced variety distribution formed by plugging  $\bar{g}$  into the PDF of a  $\text{Unif}(-\epsilon, \epsilon)$  PDF for small  $\epsilon$  provides an interesting, intuitive procedure. The PDF of the uniform distribution is always proportional to a constant over its support and zero elsewhere, so  $\tilde{p}(x, y|g, \epsilon) = 1[-\epsilon \leq \bar{g} \leq \epsilon]$ . If we use the same proposal  $q(\mathbf{x})$  that is uniform over the square  $\mathcal{X}$ , notice that we can skip the

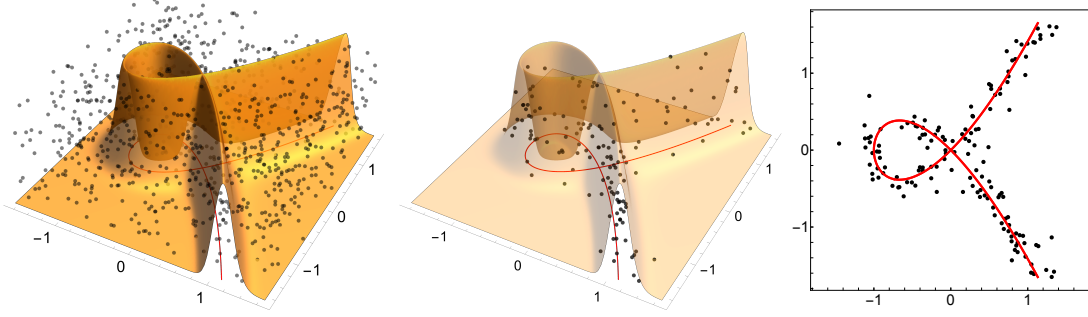


Figure 14: Rejection sampling is a simple algorithm that can be used to sample from low-dimensional variety distributions. Here we sample from the  $\mathcal{N}_{2,\mathbf{x}}(y^2 - (x^3 - x^2), \frac{1}{10^2})$  distribution using a uniform proposal distribution over  $\mathcal{X} = [-1.5, 1.5]^2$ . We begin with 10,000 points (left), of which only 1,948 were found to be under  $\tilde{p}(x, y|g, \sigma^2)$ , or about 1 in 5 draws (middle). The projected values, the  $(x, y)$  coordinates of the draws, are then retained (right). Probabilistically this corresponds to marginizing the height variable  $u$ .

uniform sampling of the auxiliary variable  $u$  entirely, since  $\tilde{p}$  is either 0 or 1. In this case, the algorithm reduces to this: 1) sample  $x, y \sim \text{Unif}(-1.5, 1.5)$ ; 2) evaluate  $\bar{g}(x, y)$ ; and 3) retain  $(x, y)$  if  $|\bar{g}(x, y)| \leq \epsilon$ . This is very similar to the naive technician’s procedure that, when looking for where  $g$  is 0, simply evaluates  $g$  at a collection of random points and retains the ones that are close to zero, but with one distinction: the present procedure uses the normalized version  $\bar{g}$ , not  $g$ , and that constitutes a significant distinction. Figure 15 illustrates this distinction on the Lissajous polynomials [Merino, 2003].

Figures 14 and 15 are very suggest that the method works very well, and it does, at least in low dimensions. It has several advantages: it produces independent draws, it is almost trivial to implement, and it is easy to monitor. But it suffers from a number of disadvantages as well. First, one needs to know a priori some sense of what the spatial extent is of the variety. It may be possible to use clever transformations to alleviate this problem, but it still presents a challenge that would likely need to be addressed on an individual basis. Second, and more serious, is scaling. For varieties in higher dimensional spaces, the variety distribution is likely to focus its mass near a very small region of the ambient space. This region becomes vanishingly small as the dimension of the problem increases. Naive uniform box-style samplers will be too inefficient to be of practical value. Perhaps more efficient rejection sampling-style schemes can be developed here, with better and perhaps even adaptive proposals, but we do not consider them further. This exact same scenario is encountered routinely in Bayesian statistics, so it is to their solutions we now turn.

#### 4.1.2 MCMC sampling

The major engine behind Bayesian sampling is Markov chain Monte Carlo (MCMC). MCMC is a class of algorithms that enable one to sample from an un-normalized distribution by constructing a Markov chain whose stationary distribution is the target distribution. To generate observations from this distribution, the chain is initialized at an arbitrary location in the support of the distribution and proceeds by iterating through proposal and acceptance steps. In the proposal step, another point in the support of the distribution is generated using a transition kernel, and in the acceptance step that proposed value is either accepted or rejected with a probability designed in such a way that the stationary distribution of the chain is the distribution of interest. In a typical setting, this probability (the Metropolis probability) is the ratio of the relative likelihoods of the proposed and current states. Consequently, the normalization factors cancel and never need to be computed. MCMC is thus ideal for situations where the distribution is only known up to a constant of proportionality, like all the distributions described in Sections 2 and 3. Another way to think of MCMC is as a stochastic mode-seeking algorithm, and this perspective in particular may help to understand the use of Hamiltonian dynamics below.

There are many schemes commonly used for MCMC. In recent years Hamiltonian Monte Carlo (HMC)



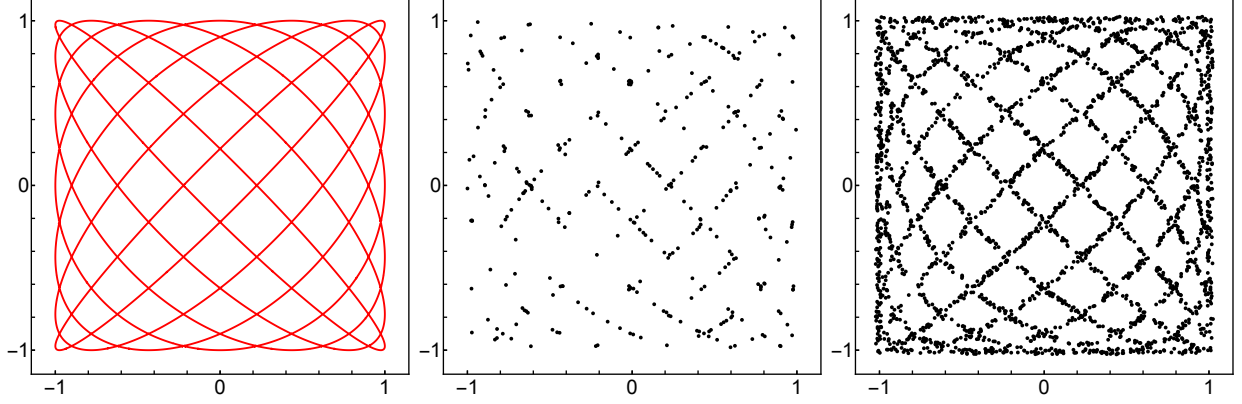


Figure 15: The rejection sampling algorithm on the induced variety distribution  $\text{Unif}(-\epsilon, \epsilon)$  on the degree-18 Lissajous polynomial’s variety with  $\epsilon = .15$ . (Left) the variety, (middle) the induced distribution plugging in  $g$ , corresponding to randomly plugging in points and checking where the polynomial is  $|g| \leq \epsilon$ , and (right) the same inserting  $\bar{g}$  instead of  $g$ . The acceptance rate changes from 3.4% to 28.3% by using  $\bar{g}$ .  $N = 10,000$ .

has proved to be a robust general purpose strategy to sample from continuous probability distributions where other MCMC algorithms, e.g. Gibbs sampling, fail [Duane et al., 1987, Neal, 2011]. HMC simulates Hamiltonian dynamics to generate proposal draws in high probability regions. The simulation is equivalent to monitoring the position of a puck imparted with a randomly generated momentum and sliding on a frictionless surface whose height is based on the negative log of the target density. Regions of high probability density are low regions on the surface, and so the puck tends to stay in them even as it slides around the irregularly shaped surface. After some time, the puck is stopped, and its location is used as the proposed value. Then the standard Metropolis probability is computed and the draw is accepted or rejected in the phase space and projected back down into the original space, much like rejection sampling. Under general conditions, as long as the Hamiltonian dynamics are simulated carefully this process leads to a Markov chain whose stationary distribution is indeed the distribution of interest. Neal [2011] is an authoritative, accessible, and freely available introduction. The process is illustrated in Figure 16.

A mathematical description of how the basic HMC algorithm works and how it applies to the variety normal distribution is helpful to understand how nicely suited it is to that task. In general, when performing HMC one constructs a Hamiltonian  $H(\mathbf{x}, \mathbf{p}) : \mathbb{R}^n \times \mathbb{R}^n \rightarrow \mathbb{R}$  that satisfies Hamilton’s equations

$$\frac{dx_i}{dt} = \frac{\partial}{\partial p_i} H(\mathbf{x}, \mathbf{p}) \quad \text{and} \quad \frac{dp_i}{dt} = -\frac{\partial}{\partial x_i} H(\mathbf{x}, \mathbf{p}).$$

Here  $\mathbf{x}$  represents the candidate draw from the distribution and  $\mathbf{p}$  a collection of auxiliary variables analogous to the single auxiliary variable  $u$  in rejection sampling. One typically assumes  $H(\mathbf{x}, \mathbf{p}) = U(\mathbf{x}) + K(\mathbf{p})$ . In the physical analogy,  $\mathbf{x}$  is the position of the puck,  $\mathbf{p}$  is its momentum,  $U(\mathbf{x})$  is its potential energy, and  $K(\mathbf{p})$  is its kinetic energy; all of these vary in time. The potential energy is related to the (potentially un-normalized) target PDF via  $U(\mathbf{x}) = -\log \tilde{p}(\mathbf{x})$ , and the momentum distribution is typically set to a multivariate normal so that  $K(\mathbf{p}) = \mathbf{p}' \mathbf{M}^{-1} \mathbf{p} / 2$ , where  $\mathbf{M}$ , the “mass matrix,” is a tuning parameter that gauges the variability of the imparted momentum, its magnitude and direction. It is usually estimated in an introductory warmup stage of running the chains, often as a scaled identity matrix, in an effort to optimize the efficiency of the sampling. In the case of the variety normal with  $n \geq m$  (at least as many variables as equations),  $\mathbf{J}_x^+ = \mathbf{J}_x' (\mathbf{J}_x \mathbf{J}_x')^{-1}$ , and the random vector  $\mathbf{X} \sim \mathcal{N}_n(\mathbf{g}, \Sigma)$  has PDF  $p(\mathbf{x}|\mathbf{g}, \Sigma) \propto \exp \left\{ -\frac{1}{2} \bar{\mathbf{g}}(\mathbf{x}|\mathbf{B})' \Sigma^{-1} \bar{\mathbf{g}}(\mathbf{x}|\mathbf{B}) \right\}$ , so

$$U(\mathbf{x}) = \frac{1}{2} \bar{\mathbf{g}}(\mathbf{x}|\mathbf{B})' \Sigma^{-1} \bar{\mathbf{g}}(\mathbf{x}|\mathbf{B}) = \frac{1}{2} \mathbf{g}(\mathbf{x}|\mathbf{B})' \left( (\mathbf{J}_x^+)' \Sigma^{-1} \mathbf{J}_x^+ \right) \mathbf{g}(\mathbf{x}|\mathbf{B}).$$

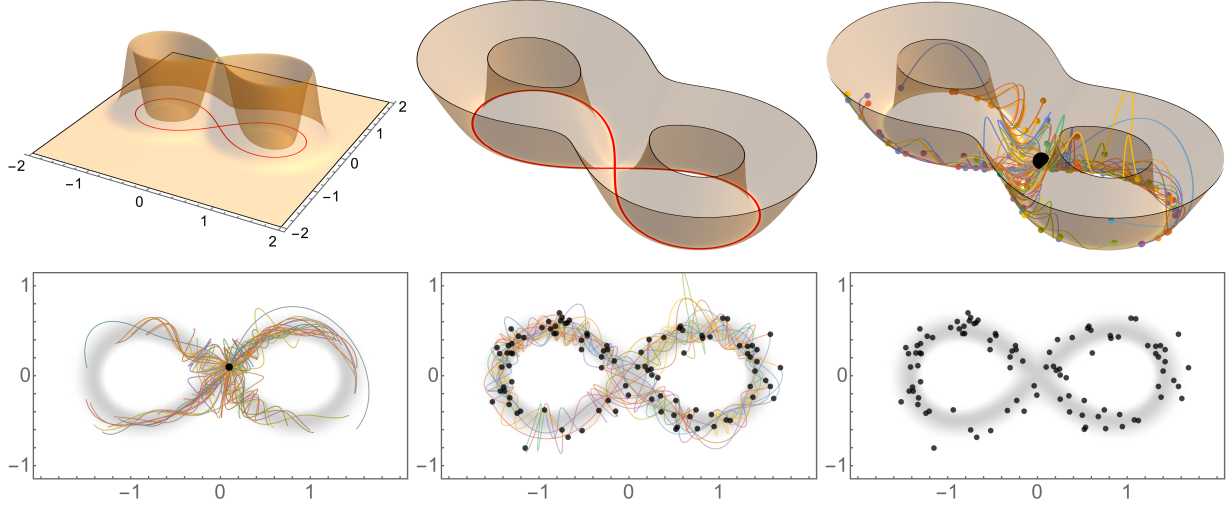


Figure 16: HMC samples distributions by simulating Hamiltonian dynamics on  $-\log \tilde{p}(\mathbf{x})$ , which allows paths to efficiently explore the distribution. This display illustrates the process for the variety normal on the polynomial  $g(x, y) = (x^2 + y^2)^2 - 2(x^2 - y^2)$ , the lemniscate of Bernoulli,  $\sigma = \frac{1}{10}$ . Top:  $\tilde{p}(\mathbf{x})$ ,  $-\log \tilde{p}(\mathbf{x})$ , and 100 different simulated paths originating from  $(.1, .1)$ . Bottom: The same 100 paths in the  $(x, y)$  plane, and a real HMC simulation using head-to-tail simulations with and without the transition paths.

If  $\Sigma = \sigma^2 \mathbf{I}_n$  as would typically be the case when exploring varieties, from (5) this further reduces to

$$U(\mathbf{x}) = \frac{1}{2\sigma^2} \mathbf{g}(\mathbf{x}|\mathbf{B})' (\mathbf{J}_{\mathbf{x}} \mathbf{J}_{\mathbf{x}}')^{-1} \mathbf{g}(\mathbf{x}|\mathbf{B}). \quad (6)$$

If  $\mathbf{M} = \sigma_m^2 \mathbf{I}_n$ , Hamilton's equations reduce to

$$\frac{dx_i}{dt} = \frac{\partial}{\partial p_i} K(\mathbf{p}) = \frac{\partial}{\partial p_i} \mathbf{p}' \mathbf{M}^{-1} \mathbf{p} / 2 = \frac{p_i}{\sigma_m^2} \quad (7)$$

$$\frac{dp_i}{dt} = -\frac{\partial}{\partial x_i} U(\mathbf{x}) = -\frac{\partial}{\partial x_i} (-\log \tilde{p}(\mathbf{x})) = -\frac{1}{2\sigma^2} \frac{\partial}{\partial x_i} \{ \mathbf{g}(\mathbf{x}|\mathbf{B})' (\mathbf{J}_{\mathbf{x}} \mathbf{J}_{\mathbf{x}}')^{-1} \mathbf{g}(\mathbf{x}|\mathbf{B}) \}. \quad (8)$$

Of course, since  $\mathbf{g} \in \mathbb{R}[\mathbf{x}]^m$  is polynomial, the computation of  $\mathbf{J}_{\mathbf{x}}$  is trivial. While in practical implementations of HMC such as Stan automatic differentiation is used because Jacobians virtually never present in closed form, for the variety normal distribution this is the typical case.

As a general purpose algorithm, HMC has a number of parameters that require tuning for the sampler to work. For example, considerable effort has been spent answering questions that speak to how long the Hamiltonian dynamics should be simulated and how time should be discretized. Since this work is not focused on novel or optimally efficient samplers, we simply recommend the defaults of the implementation used. In our case, this is the Bayesian software Stan, which implements the No-U-Turn sampler (NUTS) algorithm, a HMC variant that seeks to tune the parameters governing the Hamiltonian dynamics by leveraging the time-reversibility of the process and avoiding random walk behavior [Hoffman and Gelman, 2014].

While implementing HMC from scratch may seem daunting, a simple trick allows us to sidestep the process and use state of the art implementations from the Bayesian community. We illustrate this process with the variety normal distribution, but similar manipulations enable its use for others we well. The trick is to recognize the PDF of the variety normal distribution as the posterior distribution of an overparameterized Bayesian model. Recall that Bayes' theorem provides that in a statistical modeling scenario where the data model is  $p(\mathbf{y}|\boldsymbol{\theta})$  and the prior is  $p(\boldsymbol{\theta})$ , the posterior distribution is proportional to the product of the

likelihood and the prior, notationally  $p(\boldsymbol{\theta}|\mathbf{y}) \propto p(\mathbf{y}|\boldsymbol{\theta})p(\boldsymbol{\theta})$ . Assuming an improper flat prior  $p(\boldsymbol{\theta}) = 1$ , this is  $p(\boldsymbol{\theta}|\mathbf{y}) \propto p(\mathbf{y}|\boldsymbol{\theta})$ , which is well known to produce proper posteriors under suitable conditions, notably in the univariate normal case with  $\sigma^2$  known [Berger, 1993]. The key is to recognize the difference in notational roles. In the case of the algebraic distributions of interest, the coefficients  $\boldsymbol{\beta}$  are known and the values of  $\mathbf{x}$  are desired, which is precisely the opposite of the typical Bayesian scenario. In particular, the role of the data  $\mathbf{y}$  is played by the coefficient vector  $\boldsymbol{\beta}$ , which is known, and that of the parameter  $\boldsymbol{\theta}$  is played by the indeterminate vector  $\mathbf{x}$ . Moreover, observing that  $\bar{\mathbf{g}}(\mathbf{x}|\mathbf{B})'\boldsymbol{\Sigma}^{-1}\bar{\mathbf{g}}(\mathbf{x}|\mathbf{B}) = (\mathbf{0}_n - \bar{\mathbf{g}}(\mathbf{x}|\mathbf{B}))'\boldsymbol{\Sigma}^{-1}(\mathbf{0}_n - \bar{\mathbf{g}}(\mathbf{x}|\mathbf{B}))$ , the variety normal PDF can be thought of as the posterior distribution over the “parameter” space  $\mathbb{R}^n$  of a data model that is multivariate normal with mean  $\bar{\mathbf{g}}(\mathbf{x}|\boldsymbol{\beta})$  and known covariance  $\boldsymbol{\Sigma}$ , a flat prior on the variates  $\mathbf{x}$ , and a single observation of  $\mathbf{0}_n$ .

Stan is a free and open-source state of the art probabilistic programming language (PPL) that is both a specification language and a sampling engine that implements HMC [Carpenter et al., 2017, Stan Development Team, 2018]. From a theoretical vantage, its engine implements both NUTS and other HMC variants, including a robust automatic differentiation suite. From an applied perspective, it is cross-platform and has interfaces in most major computing environments, including R, Python, Julia, Matlab, and others, in addition to a Linux command line version. Stan largely functions as a markup language for Bayesian models that is translated into C++ and compiled before sampling. For example, an implementation used to sample from the multivariety normal distribution defined by the equations  $x^2 + y^2 + z^2 = 1$  and  $z = x + y$ , for example, might be:

```
data { real<lower=0> si; }

parameters { real x; real y; real z; }

transformed parameters {
  vector[2] g = [x^2+y^2+z^2-1, -x-y+z]';
  matrix[2,3] J = [
    [2*x, 2*y, 2*z],
    [-1, -1, 1]
  ];
}

model { target += normal_lpdf(0.00 | J' * ((J*J') \ g), si); }
```

Since the  $\boldsymbol{\beta}$  (or  $\mathbf{B}$ ) coefficients that define the polynomial(s) function as data from the Bayesian perspective, in addition to creating individual samplers for individual variety normal distributions, Stan can be used to create a single compiled binary that samples from a suitably small class of variety normal distributions. For example, here is a Stan program to sample from the variety normal distribution on a quadratic polynomial in the indeterminates  $x$  and  $y$  that can be compiled once and then simply provided different coefficients, which this framework views as data, at run-time. It limits its scope to the window  $[-5, 5]^2$ :

```
data {
  real<lower=0> si;
  real b0; real bx; real by;
  real bx2; real bxy; real by2;
}

parameters {
  real<lower=-5,upper=5> x;
  real<lower=-5,upper=5> y;
}
```

```

model {
  real g = b0 + bx*x + bx2*x^2 + bxy*x*y + by*y + by2*y^2;
  real dgx = bx + 2*bx2*x + bxy*y;
  real dgy = by + 2*by2*y + bxy*x;
  real ndg = sqrt(dgx^2 + dgy^2);
  target += normal_lpdf(0.00 | g/ndg, si);
}

```

Of course, it bears repeating that not all combinations of parameters yield varieties over the reals, so we may need to check if an apparent component corresponds to actual roots.

## 4.2 Endgames

In some cases points on the variety may be preferred to points near it. In the current situation, if  $\sigma$  is sufficiently small, the resulting points from the sampler will be close to the variety, so a sensible approach to generating points on the variety is to project the points onto it. Mathematically, if  $\mathbf{x}_0$  is a point near the variety generated by the sampler, this corresponds to solving the  $\ell_2$  optimization problem

$$\mathbf{x}^* = \operatorname{argmin}_{\mathbf{x} \in \mathcal{V}(\mathbf{g})} \|\mathbf{x} - \mathbf{x}_0\|_2 = \operatorname{argmin}_{\mathbf{x} \in \mathcal{V}(\mathbf{g})} \|\mathbf{x} - \mathbf{x}_0\|_2^2. \quad (9)$$

The solution to this problem is unique for almost all  $\mathbf{x}_0 \in \mathbb{R}^n$ .

One may consider two basic naive strategies to compute  $\mathbf{x}^*$  for which there are many variants, both theoretical and implementation-wise. First, one may consider running any nonlinear optimization algorithm on  $h(\mathbf{x}) = \mathbf{g}(\mathbf{x})' \mathbf{g}(\mathbf{x}) = \sum g_i(\mathbf{x})^2$  initialized at  $\mathbf{x}_0$ , with the intuition being that if  $\mathbf{x}_0$  is already close to being a root of  $\mathbf{g}$ , perhaps the algorithm will move  $\mathbf{x}_0$  to  $\mathbf{x}^*$ , or at least something close. For example, if  $\mathbf{x}_0 = (x_0, y_0) = (1, 1)$  is a point drawn near the variety of  $g = x^2 + y^2 - 1$  (the unit circle in  $\mathbb{R}^2$ ),  $g(x_0, y_0) \neq 0$ , but initializing gradient descent or Newton's method (say) on the polynomial  $g^2$  will find a corresponding root of  $g$ , and one might expect that root to be close to the true projection  $\mathbf{x}^* = (x^*, y^*) = (\sqrt{2}/2, \sqrt{2}/2)$ . The resulting point will definitely be on the variety, the question is whether it is in fact  $\mathbf{x}^*$ .

Alternatively, one may introduce Lagrange multipliers  $\boldsymbol{\lambda} \in \mathbb{R}^m$  for each of the  $g_i(\mathbf{x})$ 's, form the Lagrangian  $\mathcal{L}(\mathbf{x}, \boldsymbol{\lambda}) = \|\mathbf{x} - \mathbf{x}_0\|_2^2 + \boldsymbol{\lambda}' \mathbf{g}(\mathbf{x})$ , take the gradient with respect to both variables, and solve  $\nabla_{\mathbf{x}, \boldsymbol{\lambda}} \mathcal{L}(\mathbf{x}, \boldsymbol{\lambda}) = \mathbf{0}_{n+m}$ . Unfortunately, since  $\mathcal{L}(\mathbf{x}, \boldsymbol{\lambda}) \in \mathbb{R}[\mathbf{x}, \boldsymbol{\lambda}]$  is polynomial, this system is itself a system of nonlinear polynomial equations requiring solving. Again a naive strategy may be employed to solve it, but the strategy again will not exploit the very highly structured algebraic nature of the problem. Worse, it easily produces incorrect results, as illustrated in Figure 17.

The numerical algebraic geometry community has developed powerful methods based on homotopy continuation to numerically solve systems of polynomial equations [Sommese and Wampler, 2005, Bates et al., 2013]. These methods create similar systems of equations with known solutions and carefully numerically track a homotopy that deforms the solutions of one system into solutions of another. This is done through a sequence of prediction-correction steps, usually Euler steps on the Davidenko equation followed by Newton iterations. Near the end of the path, when the solutions being tracked are near the roots of the target system, the algorithms change their behavior in order to avoid numerical problems caused by potential algebraic pathologies. For example, Newton's method is well known to not achieve quadratic convergence near singular roots. These finishing algorithms are called endgames. They only track one path, unlike homotopy continuation in general which tracks one for each potential solution. In the current situation, if  $\sigma$  is sufficiently small, the resulting points from the sampler will be sufficiently close to the variety to employ endgames to move the points to the variety.

Recent advances in numerical algebraic geometry have adapted these endgames into homotopy-based critical point methods for the purpose of projecting points suitably close to a variety onto it [Griffin and Hauenstein, 2015, Brake et al., 2019]. Describing the critical points using Fritz John conditions yields the homotopy

$$\mathbf{H}(\mathbf{x}, \boldsymbol{\lambda}; t) = \begin{bmatrix} \mathbf{g}(\mathbf{x}) - t\mathbf{g}(\mathbf{x}_0) \\ \lambda_0(\mathbf{x} - \mathbf{x}_0) + \sum_{i=1}^m \lambda_i \nabla g_i(\mathbf{x}) \end{bmatrix} = \mathbf{0}_{m+n}. \quad (10)$$

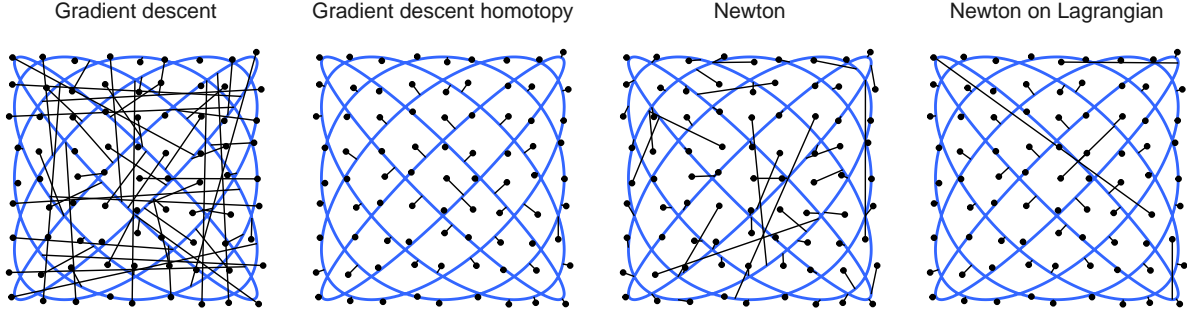


Figure 17: Points sampled from variety distributions can be projected onto them using endgames, special homotopy-based solvers that exploit the algebraic structure of the optimization problem. Naive strategies to move points to the variety can produce very unreliable results. In this image a grid of points is projected onto the degree-18 Lissajous polynomial.

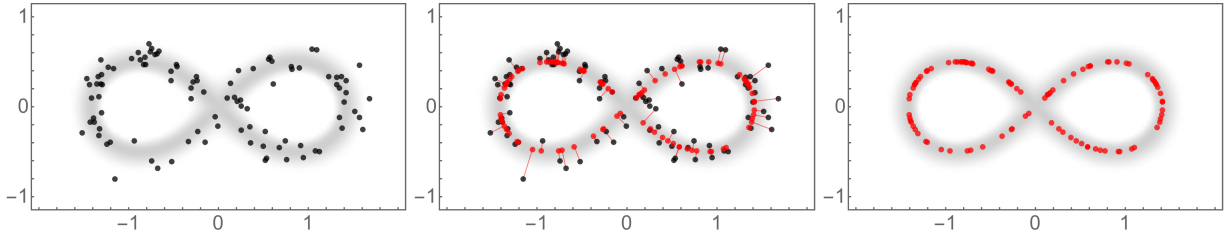


Figure 18: 100 draws from the lemniscate distribution in Figure 16 and their projections via endgames.

where  $\lambda \in \mathbb{P}^m$ , projective space of dimension  $m$ . One starts the homotopy at  $t = 1$  and start point  $(\mathbf{x}, \lambda) = (\mathbf{x}_0, [1, 0, \dots, 0])$  and aims to track to  $t = 0$ . In our case, this is most easily done using the single polynomial  $h(\mathbf{x}) = \mathbf{g}(\mathbf{x})' \mathbf{g}(\mathbf{x}) = \sum_{i=1}^m g_i(\mathbf{x})^2$  so that  $m = 1$ , and the computations can be done over an affine patch of  $\mathbb{P}^1$ , yielding the homotopy

$$\mathbf{H}^a(\mathbf{x}, \lambda; t) = \begin{bmatrix} h(\mathbf{x}) - th(\mathbf{x}_0) \\ \lambda_0(\mathbf{x} - \mathbf{x}_0) + \lambda_1 \nabla h(\mathbf{x}) \\ \lambda_0 + \alpha_1 \lambda_1 - \alpha_0 \end{bmatrix} = \mathbf{0}_{n+2}, \quad (11)$$

where  $(\alpha_0, \alpha_1)$  can be selected randomly from the standard normal distribution.

Summing up, we arrive at the following straightforward procedure: to obtain points on the variety given only its defining polynomial(s), sample from a corresponding variety distribution (usually the variety normal) and project the points onto the variety using endgames. If the variety is low-dimensional, rejection sampling is likely sufficient; otherwise, HMC via **Stan** works well. An illustration of this is included in Figure 18.

## 5 Applications

In this section we present a few applications of the methods presented in the previous sections. While we envision a broad array of potential applications, we only present three here: independence models and optimization, a model of synchronization arising from a dynamical system, and the generation of test datasets for the evaluation of various pattern recognition and machine learning tasks. In all examples we showcase

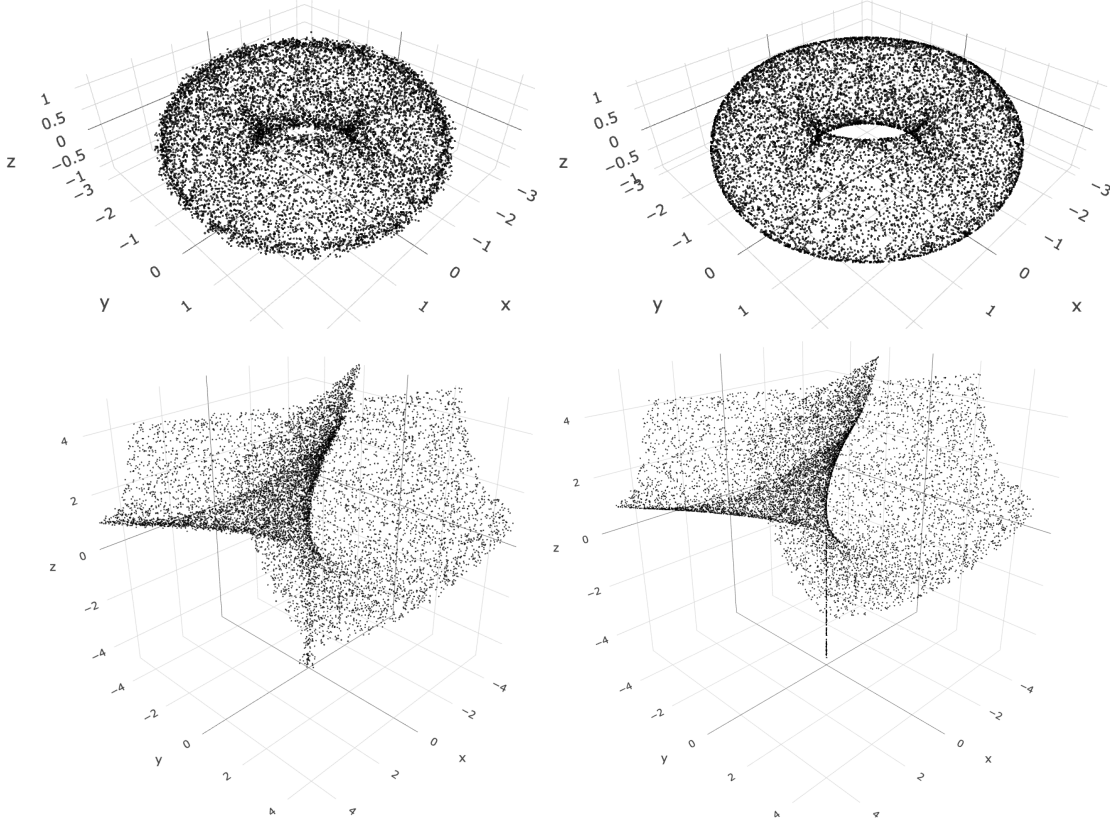


Figure 19: 10,000 draws from the torus  $g = (x^2 + y^2 + z^2 + R^2 - r^2)^2 - 4R^2(x^2 + y^2)$  with  $R = 2$  and  $r = 1$  (top) and Whitney umbrella (bottom) variety normal distributions with  $\sigma^2 = .25$  as drawn (left) and projected with endgames (right). Notice that draws are obtained on the handle and the canopy of the umbrella.

the general idea of how the methods might be used and leave any optimization or comparisons to existing methods as future work. All computations were performed in R, often using the packages **mpoly** and **algstat** [R Core Team, 2023, Kahle, 2013, Kahle et al., 2017].

## 5.1 Independence and optimization

A foundational perspective of algebraic statistics is that probabilistic independence is naturally encoded implicitly. This applies in several settings, but the most studied have been conditional independence models for multiway contingency table analysis and Gaussian graphical models [Sullivant, 2018, Drton et al., 2008]. In the latter setting, the covariance matrix is positive definite (a semialgebraic positivity constraint on the principal minors of the matrix), marginal independence is encoded as 0-covariance constraints, and conditional independence is encoded as 0 constraints on the inverse covariance matrix. The samplers from this work enable the generation of actual distributions satisfying these constraints quite easily.

A simple example of an algebraic statistical model on a contingency table is instructive. The most basic manifestation of independence is in a  $2 \times 2$  table representing two binary random variables  $X$  and  $Y$ . In this setting  $p_{ij} = P[X = i, Y = j]$  for  $i, j = 0, 1$ . By definition, independence demands four quadratic polynomial constraints  $p_{ij} = p_{i+}p_{+j}$ , where a  $+$  in the subscript indicates summing the indeterminates over the index. These are taken together with the constraint  $p_{++} = 1$  and the semialgebraic constraints  $p_{ij} \geq 0$ . As is



well known, the four independence constraints can be summarized into one:  $p_{00}p_{11} = p_{01}p_{10}$ . Ignoring the semialgebraic constraints, the model is given by  $\mathbf{g} = [p_{00}p_{11} - p_{01}p_{10}, p_{00} + p_{01} + p_{10} + p_{11} - 1] \in \mathbb{R}[\mathbf{p}]$ . 10,000 draws from the corresponding variety normal distribution with  $\sigma = .025$ , obtained via rejection sampling over the unit cube, is quite efficient. Results are shown in barycentric coordinates in Figure 20.

As in most settings, the statistical problem of estimation corresponds to an optimization problem. The feasibility region of the optimization problem in these settings is a variety and the objective function depends on the type of estimation desired [Kahle, 2011, Read and Cressie, 2012]. In the case of the  $2 \times 2$  contingency table, the empirical distribution of a dataset, the relative frequency distribution, is another point in the simplex, and its closest point on the independence surface constitutes an estimate for the model. Different distance measures describe different estimation strategies, e.g. maximum likelihood or minimum chi-square, which may or may not be algebraic in some suitable sense, e.g. polynomial, rational, etc. Numerically, solutions to the optimization problem may be obtained via a variety of different approaches, from general routines such as Newton-Raphson, iteratively reweighted least squares, or Nelder-Mead to more specialized routines such as semidefinite programming solutions or sequences thereof [Anjos and Lasserre, 2011]. In principle, variety sampling can provide a Monte Carlo scheme for such optimization problems by simply evaluating the objective function at the points sampled or (preferably) after projection. In general this is likely more useful for gaining a sense of the objective function over the variety, and not necessarily optimization itself.

As a final component of this application, one can imagine using the sampler to conduct Monte Carlo inference via inversion [Kahle, 2011]. The empirical distribution given by the relative frequency distribution of the dataset exhibits a well-known central limit theorem (CLT) used throughout categorical data analysis [Agresti, 2012]. This CLT can be used to construct an ellipsoidal confidence region around the empirical distribution. In the same way that the elementary single proportion CLT interval  $\hat{p} \pm z_{\alpha/2} \sqrt{\hat{p}(1 - \hat{p})/n}$  can be inverted to produce an asymptotically correct hypothesis test for the hypotheses  $H_0 : p \in \Theta_0$  vs.  $H_1 : p \in \Theta \setminus \Theta_0$  by simply checking for intersection with  $\Theta_0$ , this ellipsoidal region can be inverted into an inferential procedure to assess the algebraic statistical model, and precisely the same way. If enough draws are taken from the implicitly described model, operating under the reasonable assumption that they are sufficiently uniform on it, one simply has to check whether any of the points sampled falls within this ellipsoid, a trivial computation. If they do not, the procedure rejects in favor of the alternative  $H_1$  in the same way that the elementary interval does if the intersection of  $\Theta_0$  and the interval is empty.

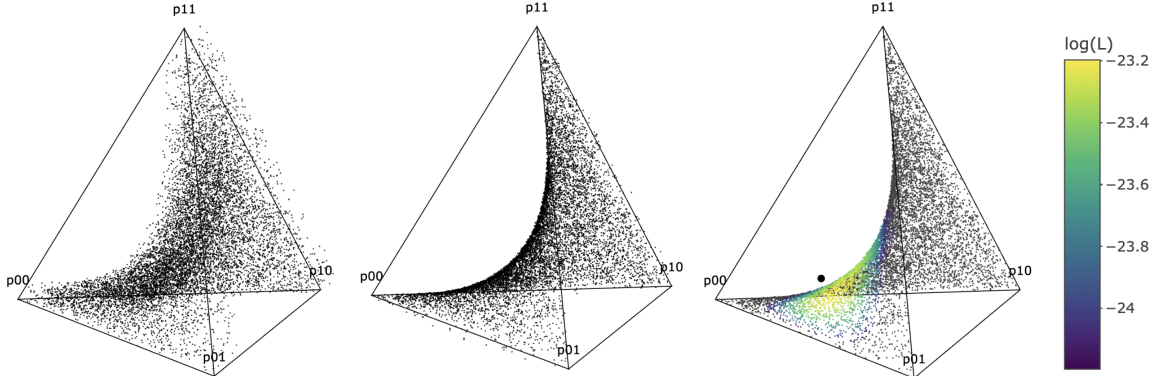


Figure 20: Independence models on contingency tables are varieties in the probability simplex that can be explored using variety distributions. Here 10,000 such distributions were sampled (left) and projected (middle) using rejection sampling. The projection took some points outside the simplex, but this could be corrected. For those inside, the log-likelihood is calculated with respect to the empirical distribution (8, 8, 1, 3), illustrating how the sampler can be used for optimization (right).

## 5.2 Exploring solutions of the Kuramoto model

Another area of intense interest in recent years has been solution sets of systems of differential equations that are polynomial and whose varieties correspond to equilibrium states. Such is the case in chemical reaction networks, for example [Gatermann, 2001, Craciun et al., 2009].

Such varieties can exhibit very interesting behavior. A commonly occurring situation for varieties arising in applications is that they decompose into components of different dimensions. Variety samplers can be applied to these situations, too, as demonstrated by computing the steady states of a dynamical system used to model synchronous behavior, namely the Kuramoto model [Kuramoto, 1975]. Following an algebraic geometrization of the Kuramoto model [Mehta et al., 2015], we demonstrate by solving the following system derived from  $N = 5$  oscillators:

$$\begin{aligned} 5s_1 - 5c_1s_2 + 5c_2s_1 - 5c_1s_3 + 5c_3s_1 - 5c_1s_4 + 5c_4s_1, & \quad 5s_2 + 5c_1s_2 - 5c_2s_1 - 5c_2s_3 + 5c_3s_2 - 5c_2s_4 + 5c_4s_2, \\ 5s_3 + 5c_1s_3 - 5c_3s_1 + 5c_2s_3 - 5c_3s_2 - 5c_3s_4 + 5c_4s_3, & \quad 5s_4 + 5c_1s_4 - 5c_4s_1 + 5c_2s_4 - 5c_4s_2 + 5c_3s_4 - 5c_4s_3, \\ c_1^2 + s_1^2 - 1, & \quad c_2^2 + s_2^2 - 1, \\ c_3^2 + s_3^2 - 1, & \quad c_4^2 + s_4^2 - 1. \end{aligned}$$

The top four describe the interaction between the oscillators, while the bottom four restrict the oscillators to the unit circle. To remove rotational symmetry, the 5<sup>th</sup> oscillator is fixed with  $s_5 = 0$  and  $c_5 = 1$ .

The system is known to have a variety in  $\mathbb{R}^8$  that consists of a 2-dimensional component and  $2^4 = 16$  points such that  $s_i = 0$  and  $c_i^2 = 1$  for  $i = 1, \dots, 4$ . Disregarding these known solutions, to understand this space of possible equilibria we sampled from the variety normal on the system and viewed the points on projection interactively. We note in passing that these points representations of varieties are easy to project since projection simply corresponds to projecting points in  $\mathbb{R}^8$  onto a linear space, and moreover projection onto coordinate axes is achieved by simply selecting component values. The results are illustrated in Figure 21 and demonstrate the power of HMC to scale variety sampling into higher dimensional spaces where rejection sampling, gridding solutions, and graphical algorithms such as marching cubes are prohibitively inefficient.

A few practical observations can be gleaned from this example.

1. As in all major MCMC schemes, HMC gets stuck in local modes when  $\sigma^2$  is sufficiently small. Variety components correspond to modes of the variety normal. Thus, some of the 64 chains migrated to and explored the 2d component while others went to different isolated solutions. As in Bayesian sampling, initializing many chains at random points, described in the Bayesian literature as “overdispersed” [Lunn et al., 2012], is prudent in an effort to discover all components.

In general there is a trade-off with respect to  $\sigma^2$  in the variety normal. The larger it is, the easier the sampling is—that is, samplers are much faster—and the less likely chains are to get stuck in disconnected components, but the fuzzier the variety appears. The smaller it is, the harder the points are to sample, but the projections of the gradient descent homotopies are more reliable. Concrete guidelines on selecting an ideal  $\sigma^2$  seems like a hard problem; however, in our limited experience with small-scale varieties getting a decent  $\sigma^2$  has been quite easy.

2. The chains ran with quite different efficiencies. While most chains finished within a second, some took a few minutes. Presumably, the chains corresponding to isolated points, which are effectively multivariate normals at those points, sampled very quickly, whereas the 2d component was explored more slowly.
3. The projections did not work perfectly, as illustrated by the stray points falling off of the isolated solutions. This was likely due to a naive implementation of the gradient descent homotopy but warrants future investigation.

We suspect that the samplers perform well in much higher dimensional settings as well, as Bayesian sampling via HMC has been applied successfully in scenarios with thousands of parameters (and more). We have not experimented with these scenarios. It should be noted that the implementation we suggest in the previous section considers each of the Jacobian elements as parameters also.

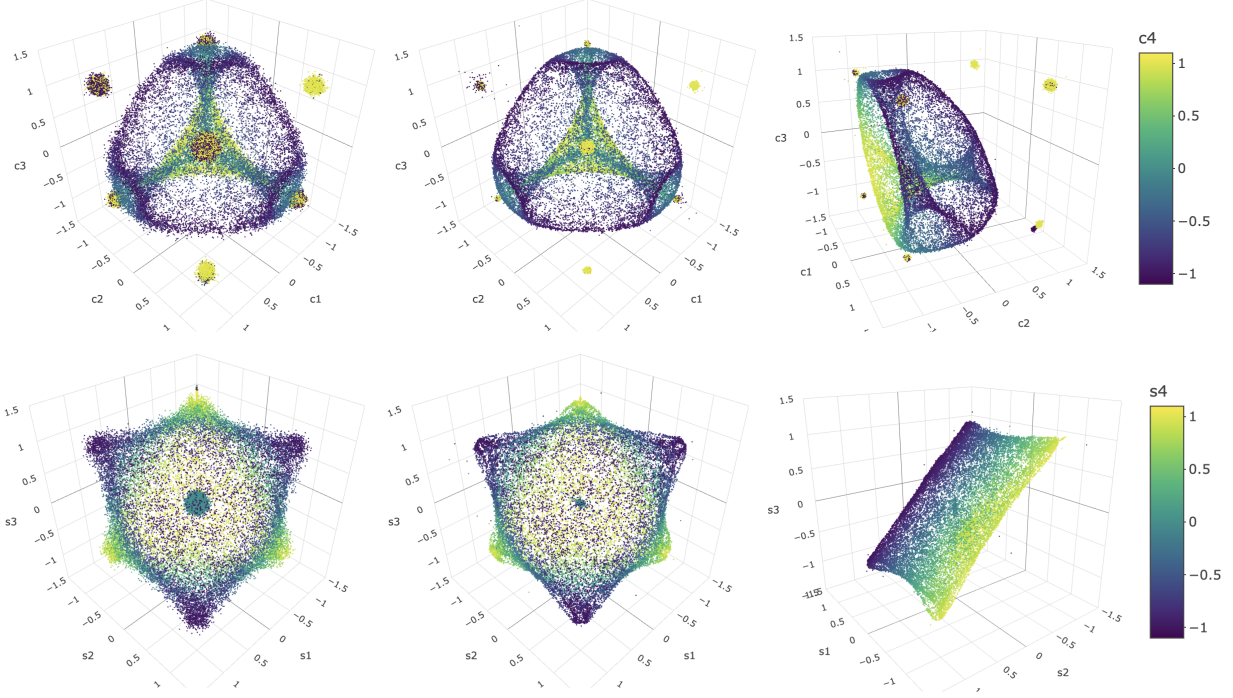


Figure 21: HMC with Stan can be effective at sampling intricate variety distributions in high dimensional settings. Here 64,000 draws from the variety normal on the  $N = 5$  Kuramoto model in 8 dimensions with  $\sigma = .05$  were drawn with 64 HMC chains in parallel. These are illustrated in projection onto  $(c_1, c_2, c_3)$  (top) and  $(s_1, s_2, s_3)$  (bottom). From left to right: raw draws, projections, and projections from a different perspective.

### 5.3 Algebraic pattern recognition and topological data analysis

In addition to providing the ability to explore varieties, the methods described in this work also admit inverse problems that generalize interpolation and regression with interesting applied math and statistical flavors. These problems typically present with a dataset (point cloud) that exhibits an algebraic structure and asks the analyst to recover that structure. For example, if in an exploratory data analysis one encounters a 2d scatterplot of points as in Figure 18, left or right, the task may be to recover the defining polynomial or some aspect thereof.

As one might suspect, these kinds of questions are not new. In the context of computer graphics, in a highly cited article [Zhang \[1997\]](#) discusses estimation methods to recover conic sections from noisy data of the form  $\mathcal{D} = \{(x_1, y_1), \dots, (x_N, y_N)\}$ . While geometrically sophisticated, the general nature of the solution is statistically routine: create a parameterized family of parametrically described conic sections and estimate the (first set of) parameters statistically. Of course, one may ask the question more generally: given  $\mathcal{D}$ , recover the algebraic curve from which the points were observed with noise. This problem is much more subtle, since (1) algebraic curves need not have parametric representations and (2) the model parameter space is not like those traditionally encountered in statistical applications. For example, two distinct polynomials may describe the same curve. The question can be stated more generally still: given a dataset  $\mathcal{D}$  of  $N$  points in  $\mathbb{R}^n$ , recover the variety from which they were observed, with or without error. The same may be considered for points in a semi-algebraic set. A similar pursuit motivated the nonlinear generalization of principal components analysis in [Vidal et al. \[2005\]](#), which has the same order of citations and has been developed into a book-length treatment [[Vidal et al., 2016](#)].

Variety distributions and samplers provide a Monte Carlo framework for experimenting with candidate solutions to these kinds of pattern recognition problems. Many areas of current interest—deep learning, manifold learning, and topological data analysis for example—seek to understand nuanced structure in point clouds; however, strategies for generating example cases to test these procedures seems to be absent from the communities and, as a consequence, one sees the same examples repeated in the literature. The distributions and samplers provided in this work seem to be excellent for this purpose. Moreover, they avoid the too-often used solution to the problem of meshing a parameter space, transporting the points to the manifold (say) via a parameterization, and adding noise. In addition to not having many such parameterized objects, the resulting clouds exhibit various oddities, from being too symmetric, in the sense of not exhibiting gaps one might expect from a randomly drawn collection of points, to being too biased to particular regions of the object of interest. These features may in fact be present in real problems, but they feel arbitrary and artefactual from a Monte Carlo perspective.

As a specific example, variety distributions seem particularly useful for experimenting with topological data analysis (TDA), which seeks to learn the topological structure of a point cloud [Carlsson, 2009]. As varieties often have interesting topological features, sampling them provides for the creation of a rich collection of synthetic datasets with which to assess TDA procedures. One of the most well-known TDA procedures, persistent homology (PH), seeks to discover topological features of point clouds of data that manifest at many different scales, e.g. holes of different dimensions. Figure 22 shows an example of the PH of draws from the degree-6 Lissajous variety normal distribution sampled via rejection sampling. PH is computed via R’s **ripserr** package, which uses the TDA software **Ripser** and plotted using **TDAvis** soon to be incorporated into **ggtda** [Wadhwa et al., 2020, Bauer, 2021, Otto and Kahle, Brunson et al., 2023]. The procedure is able to discover that the variety bounds 13 cells and to some extent is even able to speak to the relative size of those cells. This suggests that the Monte Carlo methods can feed back into (real) algebraic geometry as a tool for experimentation, possibly even providing statements about topological features (or even algebraic or geometric ones) that hold with a certain probability, akin to confidence regions.

## 6 Discussion

This article has introduced new methods to stochastically explore real algebraic and semi-algebraic sets. There are many directions to go from here; many have been suggested in other sections. In terms of the distributions in particular, a few directions would be interesting: a clearer view of when a polynomial will admit a normalizable HVN or VN; better ways to reduce the skewness for overly large dispersion  $\sigma^2$ , or even useful ways to select  $\sigma^2$  for a given  $\mathbf{g}$ ; better treatment of semi-algebraic distributions that don’t overconcentrate on the boundaries; consideration of distributions over  $\mathbb{C}^n$  (and applications); adjustments that reduce the effects of multiplicity on variability (e.g.  $g$  vs  $g^2$ ,  $g^3$ , etc.); and further investigations into which variety distributions might have special properties akin to the variety normal or variety uniform. Each of these would be fascinating and of practical utility. Similar improvements would be useful on the sampling front, including easy-to-use implementations of HMC routines for users inexperienced in that area or different strategies altogether. A thorough investigation of the samplers with large scale, or even varying scale, and complex (real) varieties would be interesting as well. We look forward to all these in the future.

In closing, one may reasonably offer the critique that most of the discussion provided in this work applies not only to varieties, but level sets of functions in general. The argument is similar to numerical continuation in the context of solving systems of algebraic equations. While it is true that the methods might work for exploring level sets of reasonably nice functions, polynomials are the primary class of such functions, mostly because the mathematics in general is more tractable with polynomials and some guarantees can be offered. For instance, it is possible to speak to normalizability to some extent over polynomials, whereas arbitrary functions  $g$  seem more challenging. In Section 4, the computations for sampling varieties are nice, unlike level sets in general, since differentiation of polynomials is nice. To check for zeros, the gradient descent homotopies are able to certify projections, theory of which depends on the underlying algebraic structure. These, combined with our own interest, has lead us to consider first and foremost zero level sets (varieties) of polynomials; however the same strategies can certainly be entertained for general functions  $\mathbf{g}$ .

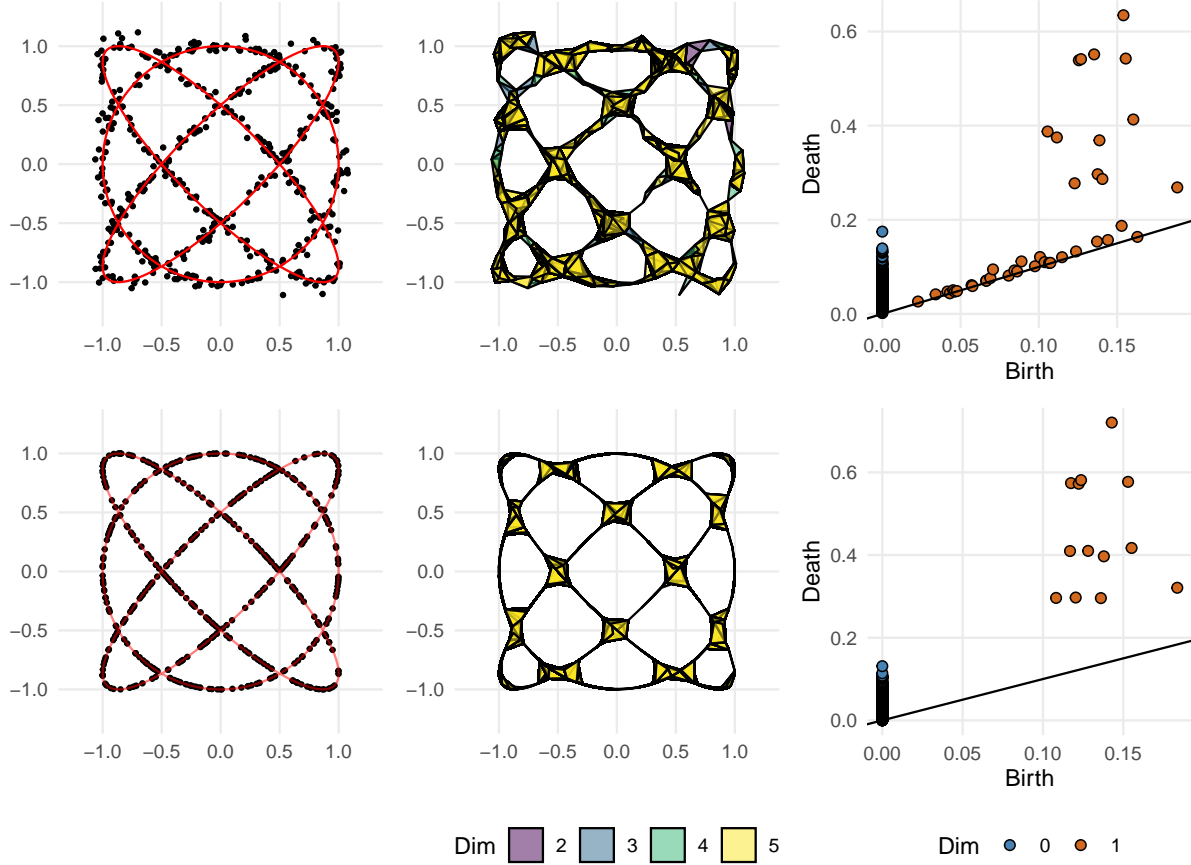


Figure 22: Variety distributions can be used for pattern recognition experiments, here TDA. A 2d point cloud, simplicial complex, and persistence diagram are illustrated using 500 draws from the degree-6 Lissajous variety normal distribution  $\mathcal{N}(9x^2 - 24x^4 + 16x^6 + 9y^2 - 24y^4 + 16y^6 - 1, \sigma = .025)$ , raw (top) and projected (bottom). Note that the 13 orange points in the persistence diagram correspond to the 13 cells bounded by the varieties; their horizontal alignment corresponds to their size being the same, showing the symmetry of the  $13 = 4 + 4 + 4 + 1$  cells. Ordinarily only the persistence diagram would be visualized.

## References

- Alan Agresti. *Categorical Data Analysis*. John Wiley & Sons, 3 edition, 2012.
- Miguel F Anjos and Jean B Lasserre. *Handbook on semidefinite, conic and polynomial optimization*, volume 166. Springer Science & Business Media, 2011.
- Daniel J Bates, Jonathan D Hauenstein, Andrew J Sommese, and Charles W Wampler. *Numerically solving polynomial systems with Bertini*, volume 25. SIAM, 2013.
- Ulrich Bauer. Ripser: efficient computation of vietoris-rips persistence barcodes. *Journal of Applied and Computational Topology*, 5(3):391–423, 2021.
- James O Berger. *Statistical decision theory and Bayesian analysis*. Springer Series in Statistics. Springer Science & Business Media, 1993.



- J. Bochnak, M. Coste, and M. Roy. *Real Algebraic Geometry*, volume 36. Springer-Verlag, 1991.
- Danielle A. Brake, Noah S. Daleo, Jonathan D. Hauenstein, and Samantha N. Sherman. Solving critical point conditions for the hamming and taxicab distances to solution sets of polynomial equations. Preprint, available at [www.nd.edu/~jhauenst/preprints/bdhsCritical.pdf](http://www.nd.edu/~jhauenst/preprints/bdhsCritical.pdf), 2019.
- Paul Breiding and Orlando Marigliano. Random points on an algebraic manifold. *SIAM Journal on Mathematics of Data Science*, 2(3):683–704, 2020.
- Jason Cory Brunson, Raoul Wadhwa, and Jacob Scott. *ggtda: 'ggplot2' Extension to Visualize Topological Persistence*, 2023. URL <https://rrrlw.github.io/ggtda/>. R package version 0.1.0.
- Gunnar Carlsson. Topology and data. *Bulletin of the American Mathematical Society*, 46(2):255–308, 2009.
- Bob Carpenter, Andrew Gelman, Matthew D Hoffman, Daniel Lee, Ben Goodrich, Michael Betancourt, Marcus Brubaker, Jiqiang Guo, Peter Li, and Allen Riddell. Stan: A probabilistic programming language. *Journal of Statistical Software*, 76(1):1–32, 2017.
- D. Cox, J. Little, and D. O’Shea. *Ideals, Varieties, and Algorithms*. Springer, New York, 2 edition, 1997.
- D. Cox, J. Little, and D. O’Shea. *Ideals, Varieties, and Algorithms: An Introduction to Computational Algebraic Geometry and Commutative Algebra*. Springer, New York, 4 edition, 2015.
- Gheorghe Craciun, Alicia Dickenstein, Anne Shiu, and Bernd Sturmfels. Toric dynamical systems. *Journal of Symbolic Computation*, 44(11):1551–1565, 2009.
- Mathias Drton, Bernd Sturmfels, and Seth Sullivant. *Lectures on algebraic statistics*, volume 39. Springer Science & Business Media, 2008.
- Simon Duane, Anthony D Kennedy, Brian J Pendleton, and Duncan Roweth. Hybrid Monte Carlo. *Physics letters B*, 195(2):216–222, 1987.
- Karin Gatermann. Counting stable solutions of sparse polynomial systems in chemistry. *Contemporary Mathematics*, 286:53–70, 2001.
- James E Gentle. *Random number generation and Monte Carlo methods*. Springer Science & Business Media, 2006.
- Zachary A. Griffin and Jonathan D. Hauenstein. Real solutions to systems of polynomial equations and parameter continuation. *Adv. Geom.*, 15(2):173–187, 2015.
- Matthew D Hoffman and Andrew Gelman. The No-U-Turn Sampler: Adaptively setting path lengths in Hamiltonian Monte Carlo. *Journal of Machine Learning Research*, 15(1):1593–1623, 2014.
- Emil Horobet and Madeleine Weinstein. Offset hypersurfaces and persistent homology of algebraic varieties. *arXiv preprint arXiv:1803.07281*, 2018.
- David Kahle. *Minimum distance estimation in categorical conditional independence models*. PhD thesis, Rice University, 2011.
- David Kahle. mpoly: Multivariate polynomials in R. *The R Journal*, 5(1):162–170, 2013. URL <https://journal.r-project.org/archive/2013-1/kahle.pdf>.
- David Kahle, Luis Garcia-Puente, and Ruriko Yoshida. *algstat: Algebraic Statistics in R*, 2017. URL <https://github.com/dkahle/algstat>. R package version 0.1.1.
- Yoshiki Kuramoto. Self-entrainment of a population of coupled non-linear oscillators. In *International Symposium on Mathematical Problems in Theoretical Physics (Kyoto Univ., Kyoto, 1975)*, volume 39 of *Lecture Notes in Phys.*, pages 420–422. Springer, Berlin, 1975.



- David Lunn, Chris Jackson, Nicky Best, Andrew Thomas, and David Spiegelhalter. *The BUGS book: A practical introduction to Bayesian analysis*. CRC press, 2012.
- Ernst W Mayr and Albert R Meyer. The complexity of the word problems for commutative semigroups and polynomial ideals. *Advances in mathematics*, 46(3):305–329, 1982.
- Dhagash Mehta, Noah S. Daleo, Florian Dörfler, and Jonathan D. Hauenstein. Algebraic geometrization of the kuramoto model: Equilibria and stability analysis. *Chaos: An Interdisciplinary Journal of Nonlinear Science*, 25(5), 2015. 053103.
- Julio Castineira Merino. Lissajous figures and chebyshev polynomials. *The College Mathematics Journal*, 34(2):122–127, 2003.
- Theodore Samuel Motzkin. The real solution set of a system of algebraic inequalities is the projection of a hypersurface in one more dimension. *Inequalities, II (Proceedings of the Second Symposium, US Air Force Academy, Colorado, 1967)*, pages 251–254, 1970.
- Radford M Neal. MCMC using Hamiltonian dynamics. In Steve Brooks, Andrew Gelman, Galen L. Jones, and Xiao-Li Meng, editors, *Handbook of Markov Chain Monte Carlo*, Handbooks of Modern Statistical Methods, chapter 5, pages 113–162. CRC Press, Boca Raton, 2011.
- Martin Ohlson, M Rauf Ahmad, and Dietrich Von Rosen. The multilinear normal distribution: Introduction and some basic properties. *Journal of Multivariate Analysis*, 113:37–47, 2013.
- James Otto and David Kahle. *TDavis: What the Package Does (One Line, Title Case)*. URL <https://github.com/jamesotto852/TDAvis>. R package version 0.0.0.9000.
- Daniel Pecker. On the elimination of algebraic inequalities. *Pacific Journal of Mathematics*, 146(2):305–314, 1990.
- R Core Team. *R: A Language and Environment for Statistical Computing*. R Foundation for Statistical Computing, Vienna, Austria, 2023. URL <https://www.R-project.org/>.
- Timothy RC Read and Noel AC Cressie. *Goodness-of-fit statistics for discrete multivariate data*. Springer Science & Business Media, 2012.
- Christian Robert and George Casella. *Monte Carlo statistical methods*. Springer Science & Business Media, 2013.
- Andrew John Sommese and Charles Weldon Wampler. *The Numerical Solution of Systems of Polynomials Arising in Engineering and Science*. World Scientific, 2005.
- Stan Development Team. RStan: the R interface to Stan, 2018. URL <http://mc-stan.org/>. R package version 2.18.2.
- Bernd Sturmfels. *Solving systems of polynomial equations*. Number 97 in CBMS Regional Conference Series in Mathematics. American Mathematical Society, 2002.
- Seth Sullivant. *Algebraic statistics*, volume 194. American Mathematical Society, 2018.
- Jan Verschelde. Algorithm 795: PHCpack: A general-purpose solver for polynomial systems by homotopy continuation. *ACM Transactions on Mathematical Software (TOMS)*, 25(2):251–276, 1999.
- Rene Vidal, Yi Ma, and Shankar Sastry. Generalized principal component analysis (GPCA). *IEEE transactions on pattern analysis and machine intelligence*, 27(12):1945–1959, 2005.
- Rene Vidal, Yi Ma, and Shankar Sastry. *Generalized principal component analysis*. Number 40 in Interdisciplinary Applied Mathematics. Springer, 2016.

Raoul Wadhwa, Matt Piekenbrock, and Jacob Scott. **ripserr**: *Calculate Persistent Homology with Ripser-Based Engines*, 2020. URL <https://CRAN.R-project.org/package=ripserr>. R package version 0.1.1.

Zhengyou Zhang. Parameter estimation techniques: A tutorial with application to conic fitting. *Image and vision Computing*, 15(1):59–76, 1997.